Title
ADSORPTION OF ENERGY IN PHOTOCATALYTIC REACTORS

Author
Somorjai, G.A.

Publication Date
1985-07-01

Lawrence Berkeley Laboratory
UNIVERSITY OF CALIFORNIA

Materials & Molecular Research Division

Presented at the NATO Conference on Fundamentals and Developments of Photocatalytic and Photoelectrochemical Processes, Erice, Italy, May 20 - June 2, 1984; and to be published in the Proceedings

ADSORPTION OF ENERGY IN PHOTOCATALYTIC REACTORS

G.A. Somorjai

July 1985

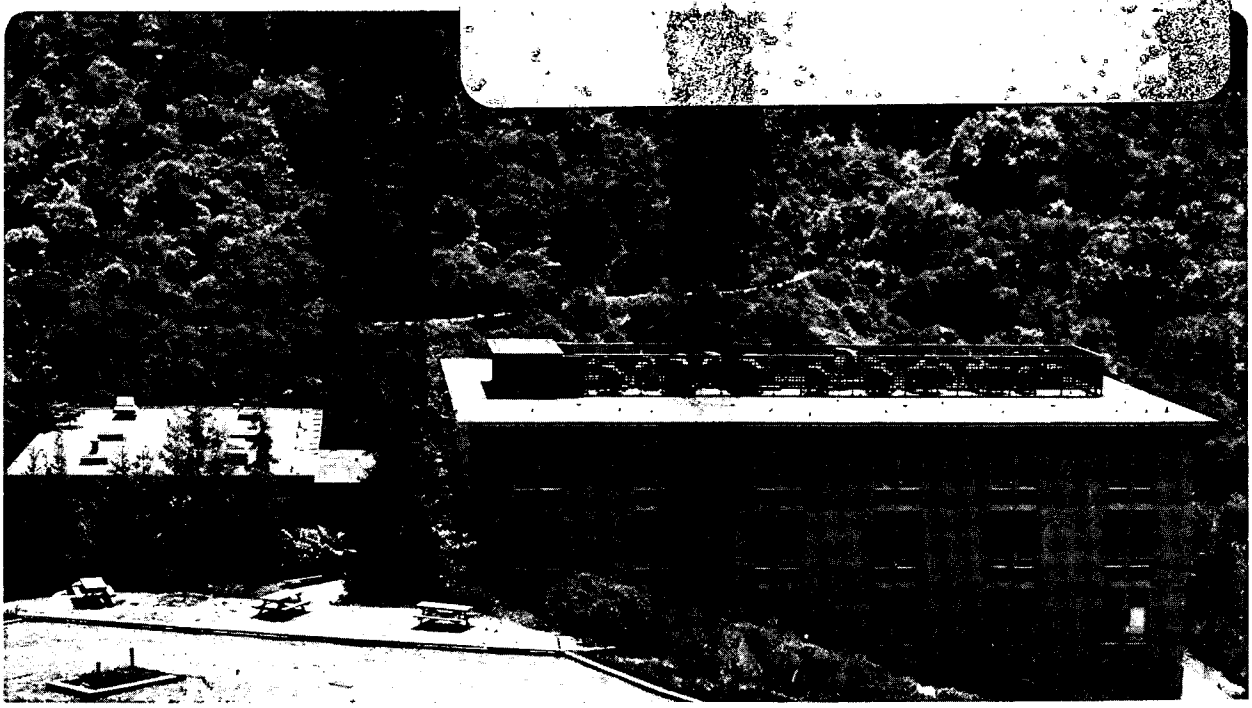

Prepared for the U.S. Department of Energy under Contract DE-AC03-76SF00098

DISCLAIMER

Adsorption of Energy in Photocatalytic Reactors

G. A. Somorjai

Materials and Molecular Research Division, Lawrence Berkeley Laboratory, and Department of Chemistry, University of California, Berkeley, CA 94720 USA

ABSTRACT

The dissociation of water to hydrogen and oxygen requires energy ΔG_{298} = 228 kJ/mole. By irradiating a semiconductor with light of energy greater than this amount, one may product electrons in the excited state and electron vacancies at the surface that can perform the photochemical reduction ($2H^+ + 2e^- \rightarrow 2H \rightarrow H_2$) and oxidation ($2OH^- + 2+ \rightarrow H_2O_2 \rightarrow H_2O + (1/2)O_2$).

There are several semiconductors, $SrTiO_3$, TiO_2, CdS, and Fe_2O_3 among them, that can photodissociate water. Some possess sites for both reduction and oxidation, while others carry out the two processes at different surfaces. A reversible solid state reaction that involves changes in the transition metal and ion oxidation state must accompany the splitting of water. Platinum, rhodium, and ruthenium oxide, when deposited on the semiconductor, serve as catalysts that accelarate the water photodissociation. These additives accelerate the recombination of hydrogen and oxygen atoms, shift the semiconductor Fermi level to a more favorable position that improves the thermodynamic feasibility for the process, accelerate electron transport, and inhibit side reactions like the photoreduction of oxygen. Many of the elementary reaction steps leading to photoproduction of hydrogen and oxygen over $SrTiO_3$ and Fe_2O_3 have been identified and will be discussed.

1. INTRODUCTION

Chemical interactions between molecules in excited electronic, vibrational, or rotational states and surfaces is a new field

of catalytic science. Until recently, catalysis of chemical reactions has only been considered for molecules in their themodyna mic ground states. Most of the surface reactions to be catalyzed were exothermic or thermodynamically downhill. In carrying out endothermic reactions, the only source of energy considered has been the addition of heat. This also assured that the molecules maintained an equilibrium energy distribution throughout the reaction.

There is growing evidence from fields other than catalysis that when molecules are allowed to react from excited electronic or vibrational states, they often take different reaction paths than would be available from a ground state configuration. Some examples of this are the deposition of materials from low energy plasmas, the formation of compounds under bombardment by high energy particles, or the application of explosions to induce bonding. Such techniques can lead to the formation of unique coatings, improved adhesion, or better electrical contact between materials.

Photoassisted thermodynamically uphill reactions such as the photodissociation of water to hydrogen and oxygen are one class of these excited state reactions. Figure 1 shows free energies for the dissociation of both H_2O and CO_2. Both of these molecules are reactants in photosynthesis to produce hydrocarbons and oxygen. If light could be used to dissociate either H_2O and CO_2, all subsequent reactions of hydrogen with carbon dioxide or carbon monoxide with water are thermodymically downhill. These reactions can readily be catalyzed by a large number of transition metals or transition metal compounds to produce small organic molecules. Thus, in the photodissociation of water for example, one produces oxygen, and the subsequent catalytic reactions of hydrogen with carbon dioxide might yield small organic molecules from inorganic photosynthesis even more efficiently than the chlorophyll-catalyzed process of photosynthesis. It is possible that inorganic photosynthesis was an important path in the formation of organic molecules in the pre-chlorophyll era of this planet.

The process of using photons to dissociate stable and abundant molecules like water and carbon dioxide could, if successful, provide for chemicals or for fuel. It is somewhat surprising how little catalytic chemistry has been published using carbon dioxide or methane as carbon sources, or using water for a source of hydrogen or oxygen.

The catalyzed photodissociation of water has been receiving increased attention since the early 70's, when the first experiments on the photoelectrochemical dissociation of water were reported.[1] When a strontium titanate ($SrTiO_3$) anode was illuminnated with light of greater than bandgap energy in a basic solution using a Pt counterelectrode, hydrogen and oxygen evolution occurred at the cathode and anode respectively without the use of any external potential.[2] The reaction was catalytic and the

electrodes showed no sign of deactivation.

The electronic state of an n-type semiconductor such as $SrTiO_3$ immersed in solution is well understood (Figure 2). Water photodissociation may also be observed when the platinum cathode is substituted with a ptype semiconductor such as gallium phosphide. In this circumstance, both the semiconductor anode and cathode must be illuminated with light of energy greater than their respective bandgaps. While both configurations may photodissociate water, these two types of photoelectrochemical cells have one essential difference. The n-type semiconductor/metal cell requires illumination of only the semiconductor anode, while the n-type/p-type semiconductor cell requires the illumination of both electrodes simultaneously to induce water photodissociation.

The thermodynamic conditions necessary to carry out this photochemical reaction have been investigated[3] and give restrictions on the location of semiconductor band edges in solution. The conduction band edge must be anodic with respect to the H^+/H_2 half reaction, while the valence band edge must be cathodic with respect to the O_2/OH^- redox couple. This way, electrons at the cathode can produce hydrogen atoms, while electron transfer from OH to hole states in the valence band will produce OH radicals, which can then be dimerized to H_2O_2, that splits up to produce oxygen.

Figure 3 shows the conduction and valence band edges for a number of oxides. In order to qualify as a suitable electrode, a material must satisfy three basic criteria. It must have a bandgap larger than 1.23 eV (ΔG for the reaction $H_2O \rightarrow OH + H^+$). In addition, band edges must be appropriately positioned with respect to the redox couples as described above. Finally, the material must be chemically stable under the reaction conditions.

As seen in Figure 3, $SrTiO_3$ satisfies the thermodynamic conditions remarkably well, while Fe_2O_3 does not. In fact, $SrTiO_3$ has been found to photodissociate water with about 5% efficiency (calculated as hydrogen energy produced divided by the total photon energy) even in the short circuit configuration as shown in Figure 4. Thus when small particles or single crystal surfaces of $SrTiO_3$ are platinized and illuminated with light of energy greater than the bandgap of 3.1 eV, the steady state evolution of hydrogen and oxygen can readily be observed. The rate of gas evolution is greater if the $SrTiO_3$ is pre-reduced in a hydrogen furnace and the electrolyte solution has a pH of 14 or greater. These findings indicate that this is not only an electrochemical process, but that water photodissociation over this material involves both photoelectrochemical and photocatalytic reactions.

Carrier generation and electron transfer at the semiconductor surface are the first of several elementary steps in the photodissociation of water. Electrons and holes are usually generated near the surface in close proximity to the solution.

Thus single crystals with high charge mobilities in the bulk are not necessarily needed. Alternatively, small particles or colloids may be utilized in a short circuit configuration to maximize the active surface area of the device. Indeed colloidal platinized TiO_2 and $SrTiO_3$ systems have been found effective for water photodissociation.[4]

In this paper, we review what is known about the photoelectrochemical dissociation of water in two different configurations the $SrTiO_3$/Pt/KOH semiconductor metal system and the n-type/p-type iron oxide photoelectrochemical diode. Both have been shown to drive the water splitting photochemical reaction without an external potential. The $SrTiO_3$ based system requires illumination by light in the near UV region ($h\nu > 3.1$ eV), while the iron oxide system can operate with light in the visible region ($h\nu > 2.3$ eV). Through the discussion of these two systems for water dissociation, we will demonstrate the accomplishments and difficulties of research in this field of inorganic photosynthesis.

2. THE $SrTiO_3$/Pt/KOH SYSTEM

Figure 5 shows the steady state evolution of hydrogen from a strontium titanate single crystal which had been pre-reduced in a hydrogen furnace, platinized and immersed in 1N KOH solution. The reaction appeared to continue indefinitely with no signs of deactivation, and from the hydrogen yield, this photoinduced process appeared to utilize about 5% of the incident photon energy that is absorbed by the solid. Upon turning off the light, the hydrogen evolution stops. In fact, some of the hydrogen and oxygen disappears due to the favorable back reaction of recombination in the dark. When bandgap radiation illuminates the surface again, the evolution of hydrogen recommences. Heating the electrolyte solution increases the rate somewhat, since the activation energy for this process is about 8 kcal/mole.

A variety of surface science techniques have been used to study the elementary steps in this photochemical surface reaction. Some of these are shown in Figure 6. Auger electron spectroscopy yields the surface composition of the stoichiometric or hydrogen furnace reduced strontium titanate. Photoelectron spectroscopy reveals the presence of Ti^{3+} formal oxidation state metal ion along with Ti^{4+} ions, while ultraviolet photoelectron spectroscopy shows a small peak near the Fermi level also associated with the presence of a Ti^{3+} ion. It is apparent that Ti^{3+} ions at the strontium titanate surface play an important role during the photodissociation reaction. Figure 7 shows the intensity of the Ti^{3+} signal as water is adsorbed on the surface in the form of D_2O and the surface is illuminated. Upon illumination, deuterium gas evolves and the Ti^{3+} signal diminishes, indicating that surface ions are being oxidized to Ti^{4+}. In the dark, oxygen desorption occurs and the surface returns to its

reduced state. Upon illumination in the presence of adsorbed water, the process repeats. Thus, it appears that the photon interaction with the surface results in an oxidation/reduction reaction, involving a charge transfer for the transition metal ion from the T^{3+} to the Ti^{4+} oxidation state, which is subsequently returned to its reduced state.

Figure 8 gives direct evidence of the solid state reaction between water and the oxide surface. When $H_2{}^{18}O$ is adsorbed on the surface and a thermal desorption experiment is carried out, part of the water desorbs as $H_2{}^{18}O$. In addition, a substantial amount of the water desorbs in the form of $H_2{}^{16}O$. This indicates ates an exchange of oxygen in the water with the oxygen in the oxide surface. Further information on this solid state reaction is provided by Figure 9, showing a thermal desorption spectrum from $SrTiO_3$ after adsorption of D_2O or D_2 on the surface. In both cases, the D_2 desorbs in addition to D_2O, indicating that the deuterium is a reducing agent which removes oxygen from the oxide lattice. From these results, one can conclude that the photodissociation of water over $SrTiO_3$ is a solid state surface reaction similar to the photographic process except that instead of a gross, irreversible photodecomposition of the solid itself, molecules near the surface undergo a reversible photodecomposition. The oxidation/reduction cycle of the transition metal ions on the surface is an integral part of this process.

In Figure 10, the importance of the presence of alkali hydroxide in this process is demonstrated. As one increases the hydroxyl ion concentration in the electrolyte solution, there is an increased rate of hydrogen evolution. Photoelectron spectroscopy indicates that the surface is completely hydroxylated. In Figure 11, the top curve shows the UPS spectrum from sodium hydroxide. The three electronic transitions are the fingerprints of the presence of OH^- ions. It is clearly seen that the strontium titanate surface in the presence of hydrogen or water shows the same fingerprint. Thus we can infer that a strontium titanate surface which is active towards water photodissociation is completely hydroxylated.

The hydroxylation of the oxide surface does not occur readily at room temperature, and the presence of potassium hydroxide or other alkali hydroxides seems to catalyze this process. This is the reason that alkali hydroxide plays such an important role when the reaction is carried out at 300K. However, if we carry out the reaction at 450-500K in the presence of steam, alkali hydroxides are not needed. Under these circumstances, the surface is readily hydroxylated and hydrogen evolution commences without the presence of alkali hydroxides.[5]

Next, we investigate the importance of the presence of platinum or other metals on the surface in accelerating this reaction. Table I indicates that the reaction occurs faster in the presence of metals on the surface. Platinum seems to be more active than gold, while gold is more active than strontium titan-

ate without any metal. Hydrogen atom recombination is one of the elementary reaction steps leading to the formation of hydrogen gas after the photodissociation of water. Strontium titanate does not carry out hydrogen atom recombination well; however, platinum is an excellent catalyst for this process. Thus, the best water splitting system would involve strontium titanate that carries out the photodissociation process, alkali hydroxides that keep the surface continuously hydroxylated, and metal that is needed for hydrogen atom recombination.

Let us summarize these important findings that indicate the complexity of this process:

(1) Irradiation by energy $h\nu > 3.1$ eV is needed to induce water photodissociation over $SrTiO_3$.

(2) Alkali hydroxides such as KOH catalyze the hydroxylation of the strontium titanate surface and facilitate water dissociation.

(3) Oxygen vacancies and the presence of Ti^{3+} at the surface are critical in the dissociation.

(4) Transition metals such as Pt at the strontium titanate surface accelerate water photodissociation by catalyzing the formation of hydrogen molecules from atoms.

These observations provide information on many of the elementary reaction steps, so one can propose a simple reaction mechanism for the photodissociaton of water on strontium titanate surfaces. This mechanism is shown schematically in Figure 12.[6] In the dark, strontium titanate consists of titanium atoms in the Ti^{4+} oxidation state. Upon illumination, a photoelectron that is generated by bandgap or higher energy radiation reduces the Ti^{4+} to Ti^{3+}. The electron vacancy takes the charge from the OH ion and converts it into a peroxide molecule that splits up oxygen. The surface is left in a reduced state that is ready to adsorb another molecule of water which reoxidizes the surface to Ti^{4+} and produces hydrogen in the process. Then, the reaction will repeat itself in a catalytic manner. This mechanism is consistent with all experimental information available on the photodissociation process over strontium titanate at present.

The difficulty with strontium titanate for the photodissociation of water is the necessity for ultraviolet radiation. Since this process works poorly with solar radiation, hydrogen generation using $SrTiO_3$ is not an economical possibility. A continued search for materials that would carry out this reaction in the solar range led us to the study of iron oxide surfaces.

3. THE N-TYPE IRON OXIDE/P-TYPE IRON OXIDE PHOTOCHEMICAL DIODE

Iron oxide has a complex phase diagram that is shown in Figure 13, consisting of at least three distinct iron-oxygen compounds. Fe_2O_3 is an intrinsic n-type semiconductor with a band gap of 2.3 eV. The divalent oxide, FeO, is a p-type semiconductor with a band gap also near 2.3 eV. The mixed oxide, Fe_3O_4, is a low resistivity compound, almost metallic. In preparing separate sites for the oxidation and reduction processes, it was necessary to enhance the n-type or p-type iron oxide behavior respectively.

Early work by Hackerman et al[7] demonstrated some of the desirable properties of iron oxide for water photodissociation. When Fe_2O_3 is used against a Pt counterelectrode, photocurrents corresponding to oxygen production are generated for an applied bias of $V_a > 700$ mV, RHE. It has been found in our laboratory that doping with Si reduces the magnitude of the bias that must be employed and increases the magnitude of the anodic photocurrents. This result motivated a systematic study of various dopants in Fe_2O_3, which showed that the introduction of Mg could yield iron oxide electrodes with p-type behavior. In preparing these p-type samples we followed a well-defined procedure that included heating the mixed oxide powders to 1400°C and then rapidly quenching them in water. The resulting material was a highly heterogeneous Mg doped iron oxide, also containing phases of magnesium ferrate ($MgFe_2O_4$) and magnesium oxide (MgO). We have found that by quenching a mixed oxide of Fe_2O_3 and MgO, we can stabilize a near surface FeO phase, which has the p-type character we need. The p-type region of the Mg-doped sample was restricted to the first few microns at the surface reflecting the conditions of formation of the FeO-phase at the surface upon rapid quenching from high temperatures (~1400°C). We have also found that the p-type FeO phase may be obtained in a thin film form without Mg doping by the use of plasma sputtering in vacuum.[7]

Individual photocurrent versus voltage characteristics for the n-type (Si doped) and p-type (Mg doped) electrodes are shown in Figure 14. For the n-type (Si doped) electrodes, anodic photocurrents due to oxygen evolution appear for $V_a > 400$ mV, RHE, while the p-type (Mg doped) electrodes yielded cathodic photocurrents corresponding to H_2 evolution of $V_a < 900$ mV, RHE. Individually, these electrodes require an external bias to sustain oxygen or hydrogen evolution under illumination when employed against a platinum counterelectrode. However, when connected in a short circuit configuration as shown in Figure 15, the p/n assembly assumes an intermediate operating bias of approximately 750 mV, RHE so that O_2 and H_2 production will occur simultaneously without external bias. The iron oxide based assembly has a photoresponse more closely matched to the solar spectrum than $SrTiO_3$. Figure 16 shows the quantum efficiency (defined as the number of chemically active electron/hole pairs

produced per incident photon) plotted versus wavelength for three different iron oxide electrodes. For the undoped Fe_2O_3 electrode, the quantum efficiency was a maximum of 0.03 at a wavelength of 3800Å. Doping with Si (Figure 16b) produced photocurrents about an order of magnitude larger than undoped Fe_2O_3, due to enchanced electronic mobility. Figure 15c shows the effect of doping with Mg. In this case, the photocurrents are cathodic, while features of the spectral response curves are very similar to both the undoped and Si doped electrodes. By examining photocurrents in the near bandgap region, one can determine the bandgap. In Figure 18, we have replotted the photocurrents from the Si doped and Mg doped electrodes as $(I_{ph}h\nu)^{1/2}$ versus photon energy $h\nu$. The linearity of these plots tells us that both n-type and p-type materials are indirect bandgap semiconductors with a bandgap of approximately 2.3 eV. These results indicate that the photoelectrochemically active component in both electrodes is most likely Fe_2O_3.

The locations of conduction and valence band edges with respect to redox couples in solution are of critical importance. To determine the location of these edges on the electrochemical scale, we performed Mott Schottky measurements in which the capacitance of the space charge layer was determined for the Si doped and Mg doped electrodes separately using a phase shift technique. In Figure 18, we use the Mott Schottky relation and plot the inverse square space charge capacitance ($1/C_{sc}^2$) versus applied potential to obtain the flatband potential from the intercept for the n-type and p-type iron oxides. In addition, one can obtain carrier types and concentrations from the slopes of these plots.

For heavily doped semiconductors such as these iron oxides, the flatband potential is nearly coincident with the band carrying the majority carriers. Thus for the n-type electrode, the measured flatband potential corresponds to the conduction band edge (E_c = 200 mV, RHE); in the p-type the flatband potential gives the valence band edge (E_v = 2300 mV, RHE). Information on flatband potentials can therefore be used to generate an energy level diagram as shown in Figure 19. This shows the interfaces between the electrolyte and the n-type or p-type surfaces. We have determined band edges from Mott Schotttky plots as described above and extrapolated using the measured bandgap (2.3 eV) to find the alternate band edges. The Fermi level was determined by connecting an operating assembly through a high impedance voltmeter to a reference electrode.

From this diagram, one can easily see how the p/n assembly operates. Upon illumination in solution, electron hole pairs are produced in both the p-type and n-type iron oxides. In the p-type electrode, electrons are driven through the depletion layer towards the interface where they convert hydronium ions in solution to hydrogen gas. Conversely, vacancies driven to the n-type interface convert hydroxyl species to oxygen gas. In both

electrodes, the majority carriers migrate away from the surface to produce the observed photocurrents. Thus hydrogen evolution occurs at the p-type electrode and oxygen evolution takes place at the n-type electrode.

Hydrogen generation over undoped Fe_2O_3 was shown to be energetically unfeasible. However, in this p/n assembly, H_2 evolution now occurs readily at the p-type electrode. It appears that doping the iron oxide with Mg has shifted the p-type band edges cathodically by several hundred millivolts so that hydrogen evolution is thermodynamically feasible.

To establish that the iron oxide assembly operates as a true p/n diode with a depletion layer at both interfaces, experiments were performed using a CW Kr^+ laser. Both p-type and n-type electrodes were illuminated with the laser at a wavelength of 411 nm or 544 nm. Figure 20 shows the open circuit voltage generated between the p-type and n-type electrodes in solution as a function of illumination intensity at both wavelengths. The most important result from this plot is that open circuit voltage increases 118 mV per decade increase in light intensity. For a single depletion layer, it is known that V_{oc} will increase 59 mV for every tenfold increase in the intensity of illumination as the semiconductor is driven toward flatband conditions. Since we obtained twice this value in our experiments, it is clear that Schottky barriers exist at both the p-type and n-type electrode surfaces.

In separate experiments, oxygen evolution has been observed from an unbiased p/n cell. An $NaOH/H_2O$ solution containing isotopically labelled water ($H_2{}^{18}O$) was used as the electrolyte and the production of $^{34}O_2$ was monitored as a function of time with a mass spectrometer. Figure 21 clearly shows that oxygen was evolved when the p-type and n-type iron oxide electrodes were connected and illuminated in solution, but that no oxygen was produced when the electrodes were disconnected.

Another important consideration for the viability of this process for solar energy conversion is the long term stability of these oxides in solution. Figure 22 shows the photocurrents generated by an illuminated p-type/n-type iron oxide assembly as a function of time after the first immersion in solution. Initially, photocurrents and the corresponding gas production rates were low. However these photocurrents gradually increased over an 80 hour period to approximately 15μA, where they remained for the duration of the test. The stability of the photocurrents as well as Auger analysis of the electrodes before and after testing indicate that there is no appreciable dissolution of the iron oxide electrodes.

At present, the efficiency of the iron oxide p/n assembly is low, approximately 0.1%. This efficiency is lower than strontium titanate under ultraviolet illumination, but the iron oxide assembly operates with visible light in the solar range. In addition, iron oxide is an excellent catalyst. Thus, once hydro-

gen is created, it might be reacted in situ with carbon dioxide or nitrogen to form organic molecules or ammonia, respectively.

It is interesting to note that the olivins which comprise over 50% of the mantle of the earth have chemical compositions very similar to the doped iron oxides we have prepared. These materials are primarily iron silicates and magnesium iron silicates, which in various compounds are known to display either n-type or p-type behavior. One can speculate that some of these minerals could form p/n diode configurations, leading to the formation of hydrogen and oxygen from water in the presence of sunlight. Subsequent chemical reactions involving hydrogen might have produced organic molecules in a thermodynamically downhill process.

APPENDIX

Photoelectrochemical cells for the conversion of solar radiation to chemical are of two types: a semiconductor photoelectrode (usually an n-type anode) coupled with a metal (usually Pt) cathode, or a cell in which both the anode and cathode are illuminated semiconductors. We present theoretical maximum obtainable efficiencies for an iron oxide based system in either configuration. A comparison of efficiencies, obtained as a function of the applied potential difference between the two electrodes shows that a short circuited p/n diode assembly is the more efficient method for producing hydrogen.

Energy level diagrams are presented for both configurations, Figure 23. For the single electrode system, we consider an n-type doped α-Fe_2O_3 electrode with V_{fb} = 200mV (RHE) and E_g = 2.3eV. The band edges at the semiconductor/electrolyte interface are assumed to remain fixed. Since the conduction band edge of the n-type electrode lies anodic of the H^+/H_2 redox couple, an applied bias between the metal electrode and the semiconductor of $V_a \geq 0.2V$ is needed for the photodissociation process to begin. As the potential difference between the two electrodes is increased, the valence and conduction bands will bend in the direction of the arrows as shown in Figures 23a and 23b.

The two semiconductor electrode system shown in Figure 23b considers an n-type α-Fe_2O_3 electrode against a p-type α-Fe_2O_3 electrode with flatband potentials of 200mV and 2300mV respectively. For simplicity, we presume equal and opposite band bending on the two electrodes, and assume that the donor and acceptor densities are also equivalent. This yields identical depletion layer which were chosen to be constant, W_d = 1000Å.

Following arguments from Scaife[8], the total photocurrent from an illuminated semiconductor is

$$J_T = \int_{Eg/h}^{\infty} e\phi(\nu)(1-\exp(-\alpha(\nu)W_d V_{bb}^{1/2}))\, d\nu \quad (1)$$

where $\phi(\nu)$ is the solar flux at frequency ν(12), $\alpha(\nu)$ is the absorptivity for iron oxide[9], W_d is the depletion layer width, and V_{bb} is the amount of band bending near the semiconductor/electrolyte interface. If the solar energy conversion efficiency is defined as

$$\eta = \frac{\text{Net energy extracted}}{\text{Solar energy input}} \qquad (2)$$

then a simple expression for this efficiency when the energy is stored as hydrogen is given by

$$\eta = (1.23 - V_a)J_T/E_T \qquad (3)$$

using an integrated solar flux (12) of $E_T = 83 mW/cm^2$. Here we have included a term accounting for energy expended ($-V_aJ_T$) to maintain the external bias. A comparison of limiting efficiencies for one and two electrode assemblies of iron oxide at various applied potentials is shown in Figure 24. The iron oxide p/n assembly has a potentially greater solar conversion efficiency than the semiconductor/metal electrode system. The p/n assembly has an optimal efficiency of almost 14%, while the best to be expected from the other system is about 5%. Reasons for this are clear. In our idealized model, it is the degree of band bending which determines the ultimate efficiency. The p/n assembly offers substantial band bending of greater than one volt even without applied potential. The n-type iron oxide against a Pt cathode, however, requires considerable bias to achieve the same effect.

While regulating the potential difference between the two electrodes improves the efficiency of the single electrode system up to $V_a = 0.6$ volts, the application of external bias as shown in Figure 24 does not improve the efficiency of the p/n assembly. Band bending is already so large that additional bending provided by the external potential increases the maximum obtainable photocurrent only slightly. In fact, the net efficiency actually decreases due to the energy input required to maintain this potential.

It should be emphasized that efficiencies calculated here are theoretical maxima, and will not likely be attained in operating systems. In practice, other factors including reflection losses, surface and bulk recombination, and surface state effects will reduce these efficiencies. It does appear that in many situations p/n assemblies will offer efficiencies greater than biased semiconductor-metal electrode cells.

ACKNOWLEDGEMENTS

This work was supported by the Director, Office of Energy Re-

search, Office of Basic Energy Sciences, Chemical Sciences Division of the U.S. Department of Energy under contract No. DE-AC03-76SF00098.

FIGURE CAPTIONS

Figure 1 — Free energies for the dissociation of H_2O and Co_2 related to the electrochemical energy scale (RHE).

Figure 2 — Solid state models of band bending for n-type and p-type semiconductor electrodes immersed in aqueous solution. a) n-type semiconductor electrode short circuited to a Pt electrode, b) n-type (TiO_2) electrode in electrical contact with a p-type (GaP) electrode.

Figure 3 — Location of conduction and valence band edges of oxide semiconductors relative to the hydrogen and oxygen redox couples.

Figure 4 — Photoelectrolysis with suspensions of catalyst coated semiconductor particles.

Figure 5 — Steady state hydrogen evolution from a platinized strontium titanium (reduced) crystal immersed in 1N KOH.

Figure 6 — Surface analyses of reduced $SrTiO_3$:Ti:O ratios determined by Auger electron spectroscopy, and the presence of Ti^{3+} and Ti^{4+} ions determined by X-ray photoelectron spectroscopy and ultraviolet photoelectron spectroscopy.

Figure 7 — Simultaneous evolution of D_2 gas and the oxidation of Ti^{3+} to Ti^{4+} after water (D_2O) adsorption is shown by monitoring the D_2 gas by mass spectrometry and the intensity of the Ti^{3+} signal with ELS.

Figure 8 — Thermal desorption of water following adsorption of isotopically labelled water ($H_2^{18}O$) on a $SrTiO_3$ crystal.

Figure 9 — Thermal desorption from $SrTiO_3$ following adosrption of D_2O or D_2.

Figure 10 — Hydrogen evolution from a $SrTiO_3$/Pt. Dependence on hydroxyl concentration in the electrolyte solution.

Figure 11 The same characteristic features are seen by comparison of the UPS spectra of hydroxyl ions and $SrTiO_3$ exposed to hydrogen or water.

Figure 12 A simple reaction mechanism for the photodissociation of water on strontium titanate surfaces.

Figure 13 Iron-oxygen phase diagram.

Figure 14 Photocurrents for n-type (Si-doped) and p-type (Mg-doped) iron oxide electrodes under biased conditions.

Figure 15 Schematic illustration of p/n assembly for the photo dissociation of water using doped iron oxide electrodes.

Figure 16 Measured quantum efficiencies as a function of wavelength for doped and pure iron oxide.

Figure 17 Bandgap determinations of doped iron oxide electrodes from photocurrent dependence on wavelength.

Figure 18 Mott-Schottky plots of the inverse square of space charge capacitance versus applied potential for n-type and p-type iron oxide electrodes.

Figure 19 Energy level diagram depicting band edge locations of doped iron oxide electrodes relative to hydrogen/oxygen redox couples.

Figure 20 Open circuit voltage generated between p-type and n-type electrodes immersed in solution as a function of illumination intensity at 411nm and 544nm.

Figure 21 Oxygen evolution from a p/n assembly with doped iron oxide electrodes.

Figure 22 Photocurrent as a function of time for a p/n assembly during the first immersion.

Figure 23 Energy level diagrams for a) a single semiconductor electrode metal electrode system and b) a semiconductor/semiconductor electrode system.

Figure 24 Solar conversion efficiencies as a function of applied potential (V_a) between the electrodes.

Table I A summary of hydrogen evolution rates from stoichio-

metric and pre-reduced $SrTiO_3$ crystals in varied NaOH environments and with metal catalysts deposited on the surface.

6. REFERENCES

(1) Fujishima, A., and Honda, D., 1971, Bull. Chem. Soc. Japan 44, pp. 1148, and 1972, Nature (London), pp. 37.

(2) Wagner, F.T., and Somorjai, G.A., 1980, J. Amer. Chem. Soc. 102, pp. 5494.

(3) Gerischer, H., in Solar Energy Conversion, Topics in Applied Physics, v. 31, B.O. Seraphin, editor, 1979, Springer-Verlag.

(4) Kawai, T., ad Sakata, T., 1980, J. Chem. Soc. Chem. Comm., pp. 694.

(5) Carr, R.G., and Somorjai, G.A., 1981, Nature 290, pp. 576.

(6) Van Damme, H., and Hall, W.K., 1979, J. Amer. Chem. Soc. 101, pp. 4373.

(7) Wilhelm, J.M., Yun, K.S., Ballenger, L.W., and Hackerman, N., 1979, J. Electrochem. Soc. 126, pp. 419.

(8) Scaife, D.E., 1980, Solar Energy 21, pp. 41.

(9) Vernon, R.C., 1962, J. Appl. Phys. 33, pp. 2140.

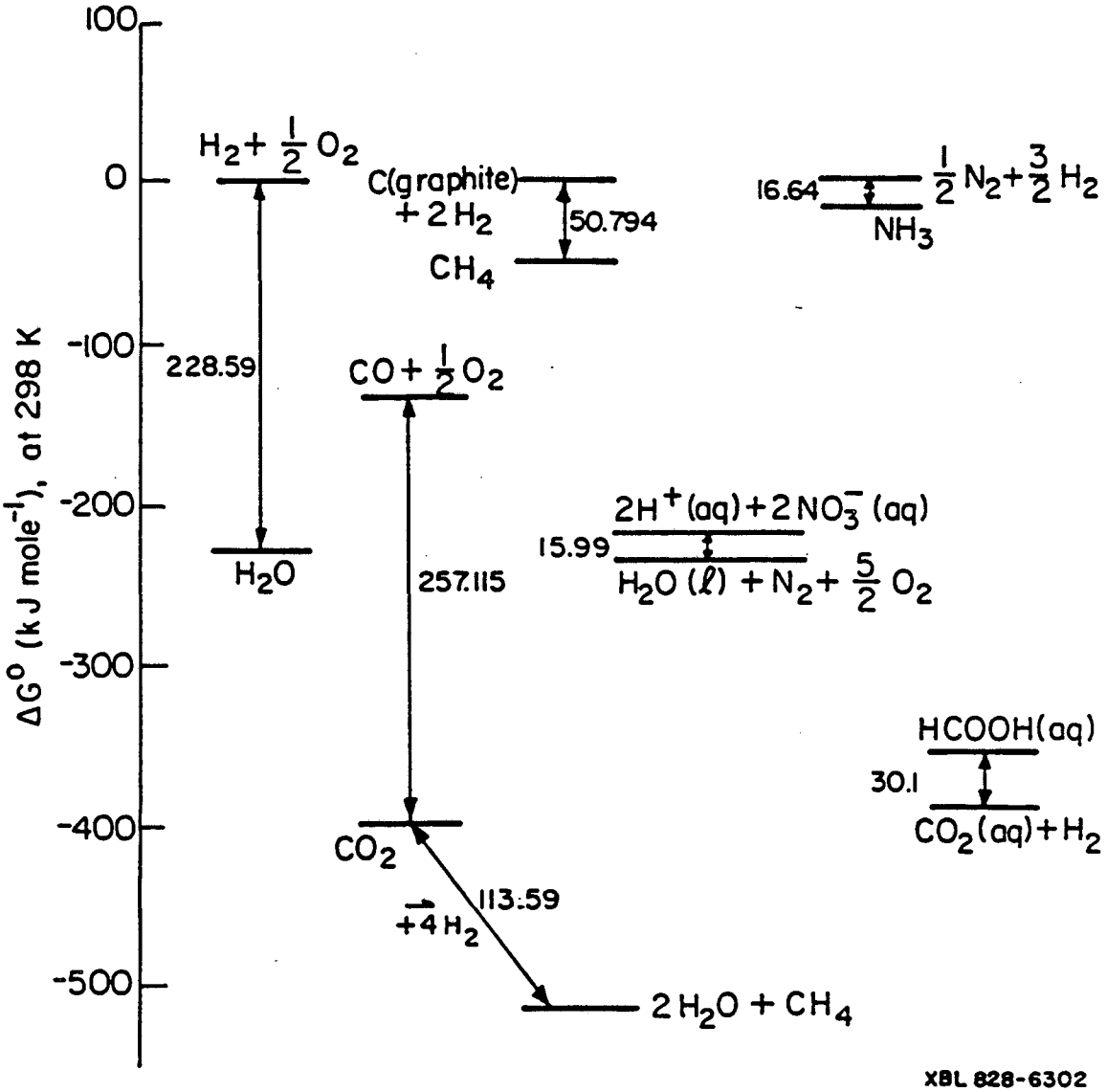
100
0
-100
-200
-300
-400
-500
ΔG° (kJ mole⁻¹), at 298 K
H2 + ½ O2
H2O
228.59
C(graphite) + 2 H2
CH4
50.794
CO + ½ O2
257.115
CO2
+4 H2
113.59
2 H2O + CH4
16.64
½ N2 + 3/2 H2
NH3
2H+(aq) + 2NO3−(aq)
15.99
H2O (ℓ) + N2 + 5/2 O2
HCOOH(aq)
30.1
CO2(aq) + H2
XBL 828-6302

Fig. 1

$$H_2O \longrightarrow H_2 + \frac{1}{2} O_2 \qquad \Delta E = 1.23\ eV$$

Semiconductor – Conductor Cell

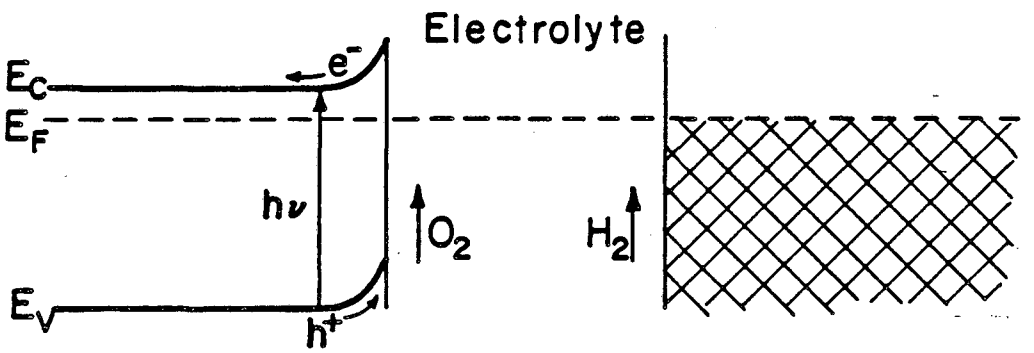

Anode
n-type Semiconductor
(TiO_2; $SrTiO_3$)

Cathode
(Pt)

Semiconductor – Semiconductor Cell

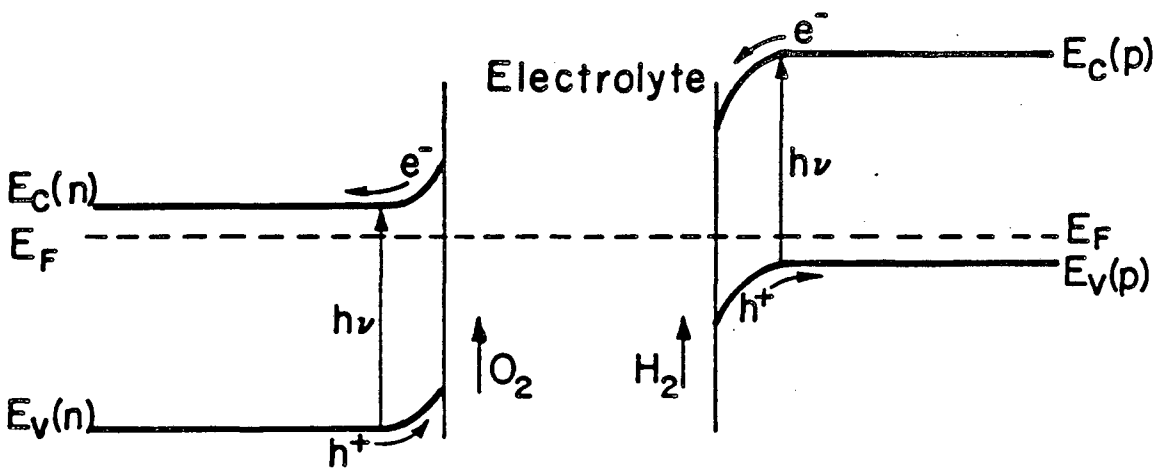

Anode
n-type Semiconductor
(TiO_2)

Cathode
p-type Semiconductor
(GaP)

XBL 7610-7610

Fig. 2

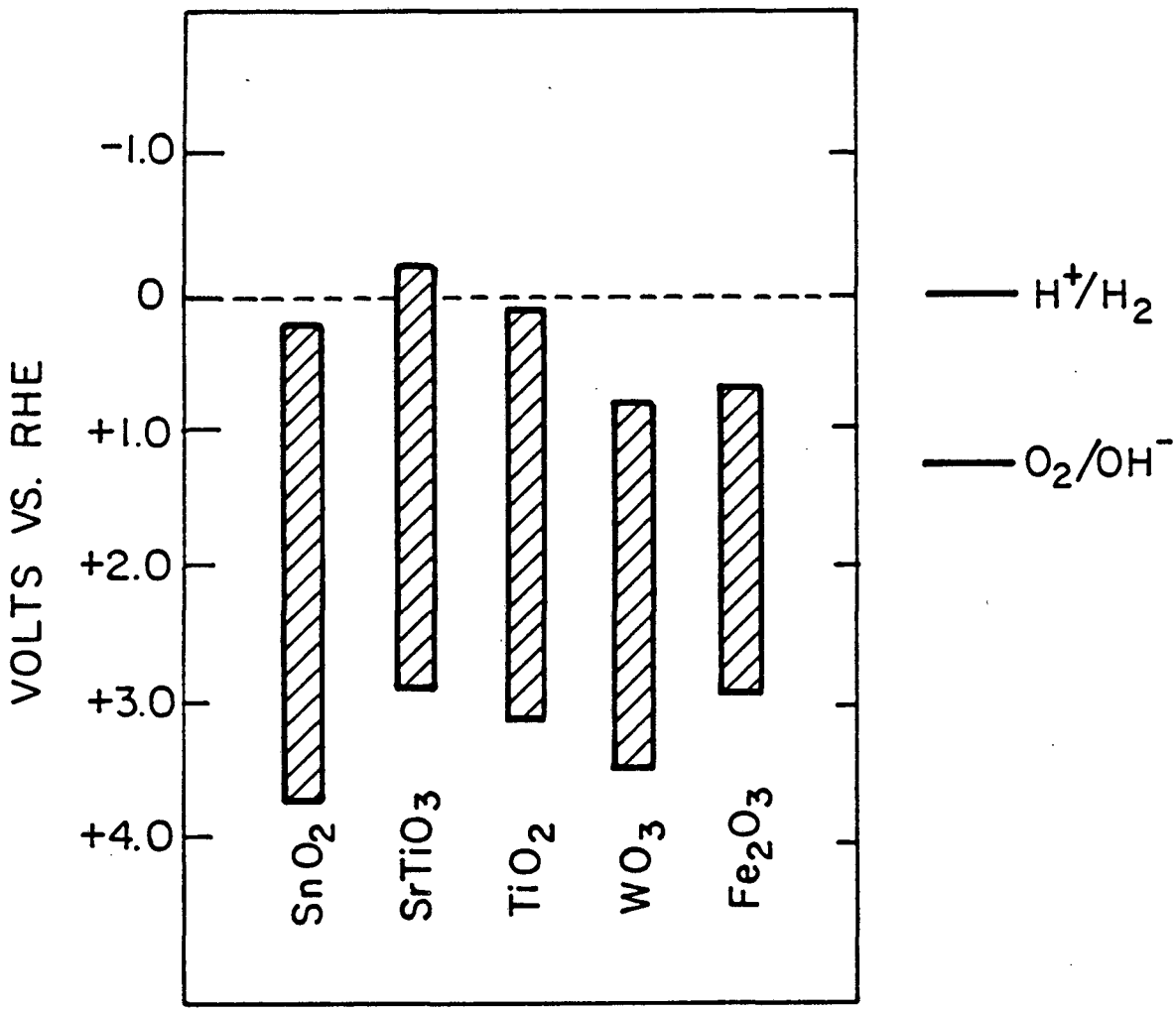
VOLTS VS. RHE
-1.0
0
+1.0
+2.0
+3.0
+4.0
SnO_2
$SrTiO_3$
TiO_2
WO_3
Fe_2O_3
H^+/H_2
O_2/OH^-
XBL 825-5829

Fig. 3

PHOTOELECTROLYSIS WITH SUSPENSIONS OF CATALYST COATED SEMICONDUCTOR PARTICLES

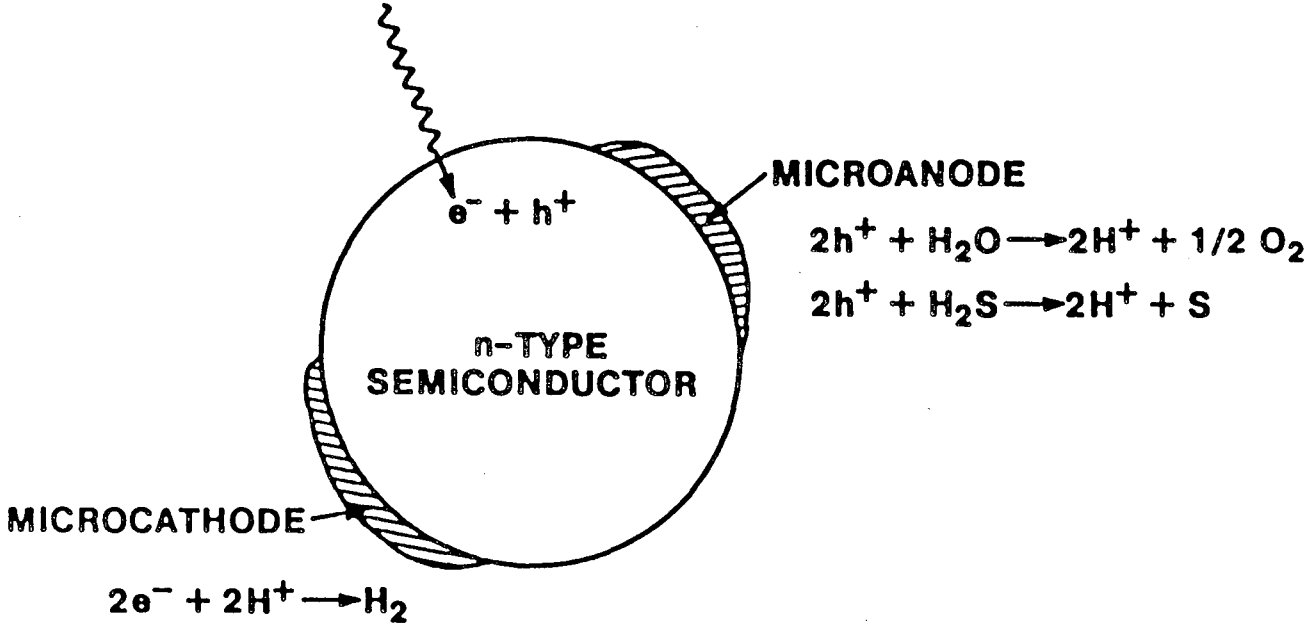

$$H_2O \rightarrow H_2 + 1/2\ O_2 \qquad \Delta V = \frac{\Delta G}{nF} = 1.23\ eV$$

$$H_2S \rightarrow H_2 + S \qquad \Delta V = \frac{\Delta G}{nF} = 0.14\ eV$$

Fig. 4

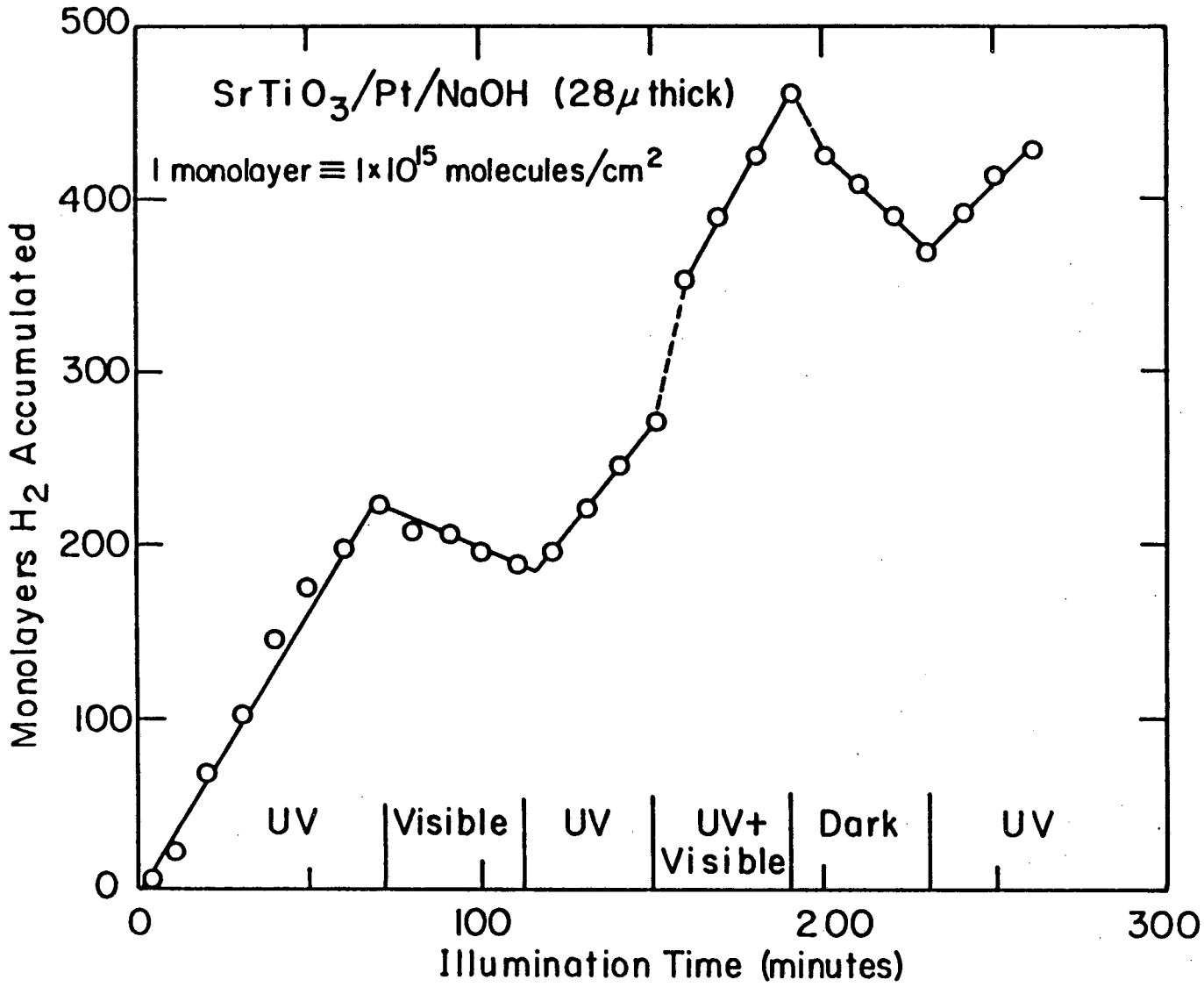

XBL 799-7067

Fig. 5

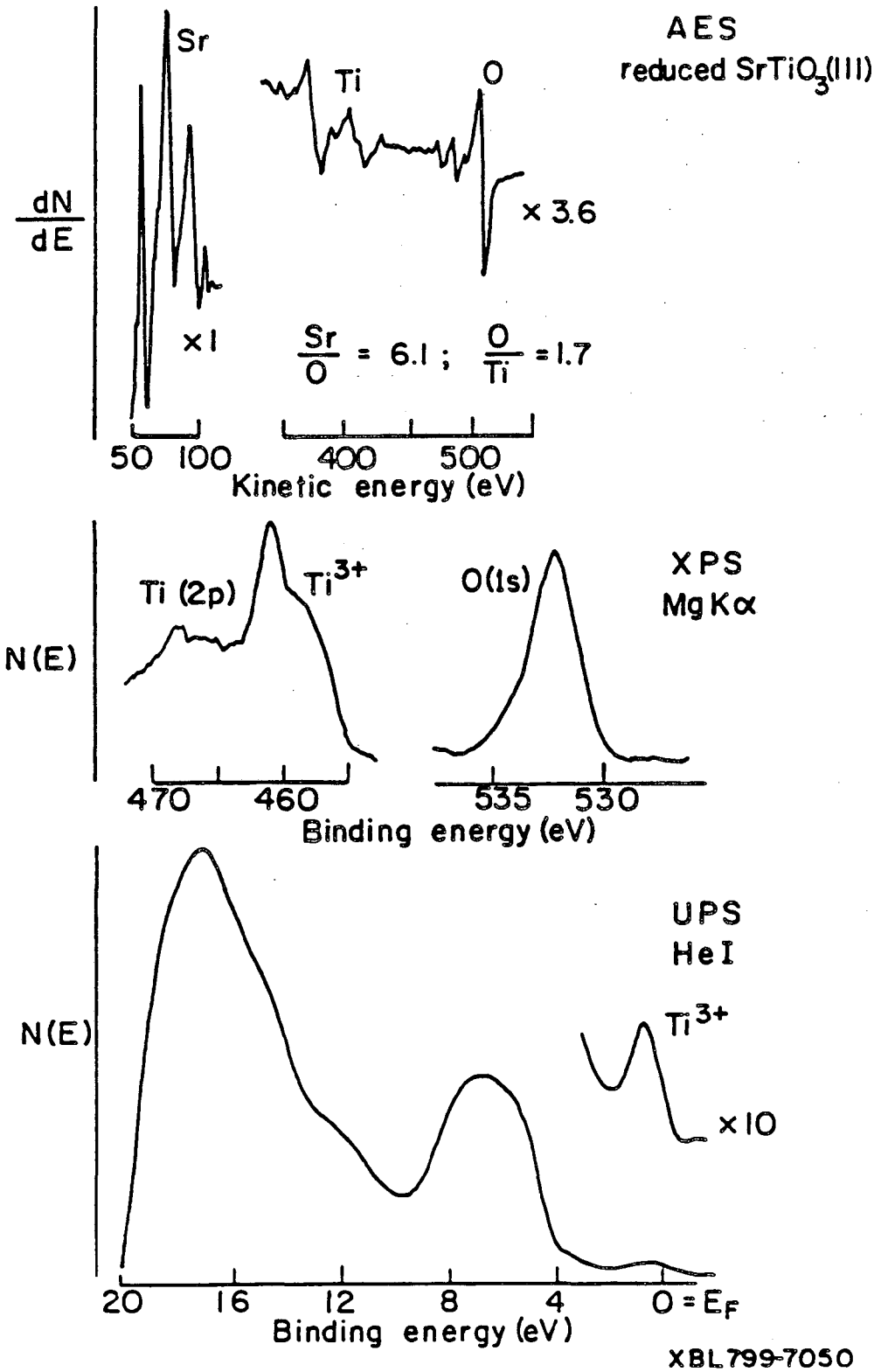
AES
reduced SrTiO3(111)
Sr
Ti
O
× 3.6
dN/dE
× 1
Sr/O = 6.1 ; O/Ti = 1.7
50 100
400 500
Kinetic energy (eV)
XPS
Mg Kα
Ti (2p)
Ti3+
O(1s)
N(E)
470 460
535 530
Binding energy (eV)
UPS
He I
Ti3+
× 10
N(E)
20 16 12 8 4 0 = EF
Binding energy (eV)
XBL 799-7050

Fig. 6

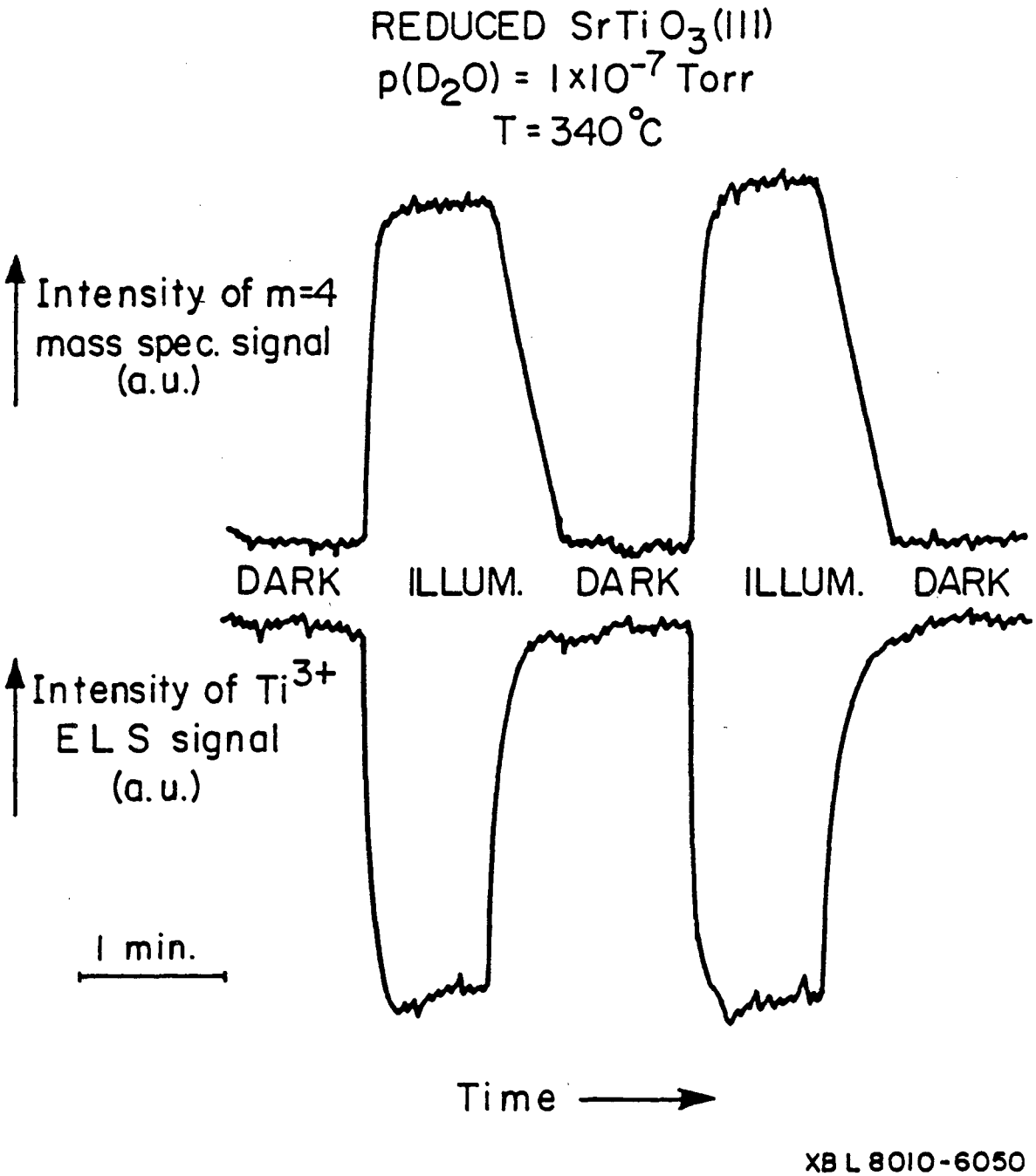
REDUCED $SrTiO_3$(111)
$p(D_2O) = 1 \times 10^{-7}$ Torr
T = 340°C
Intensity of m=4 mass spec. signal (a.u.)
DARK
ILLUM.
DARK
ILLUM.
DARK
Intensity of Ti^{3+} ELS signal (a.u.)
1 min.
Time
XBL 8010-6050

Fig. 7

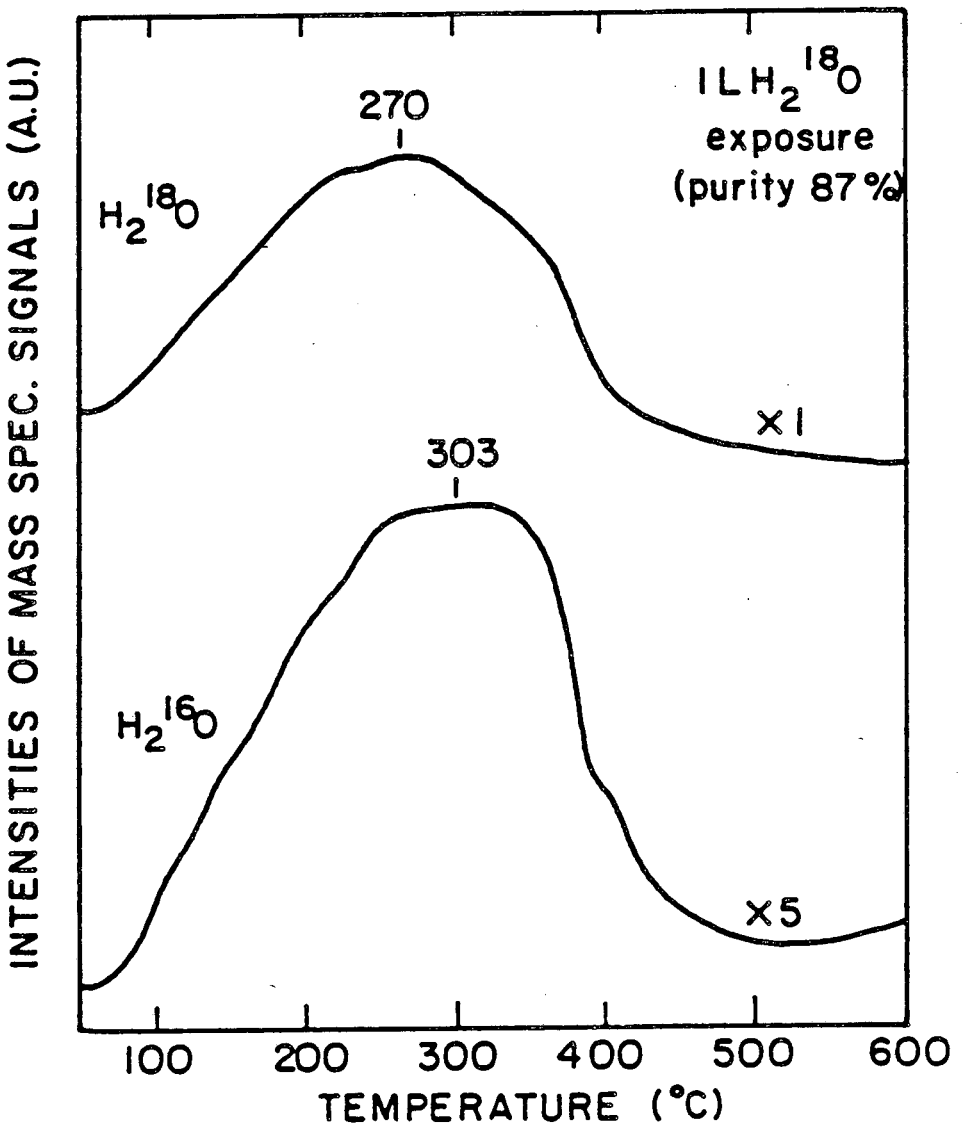

XBL 803-4762

Fig. 8

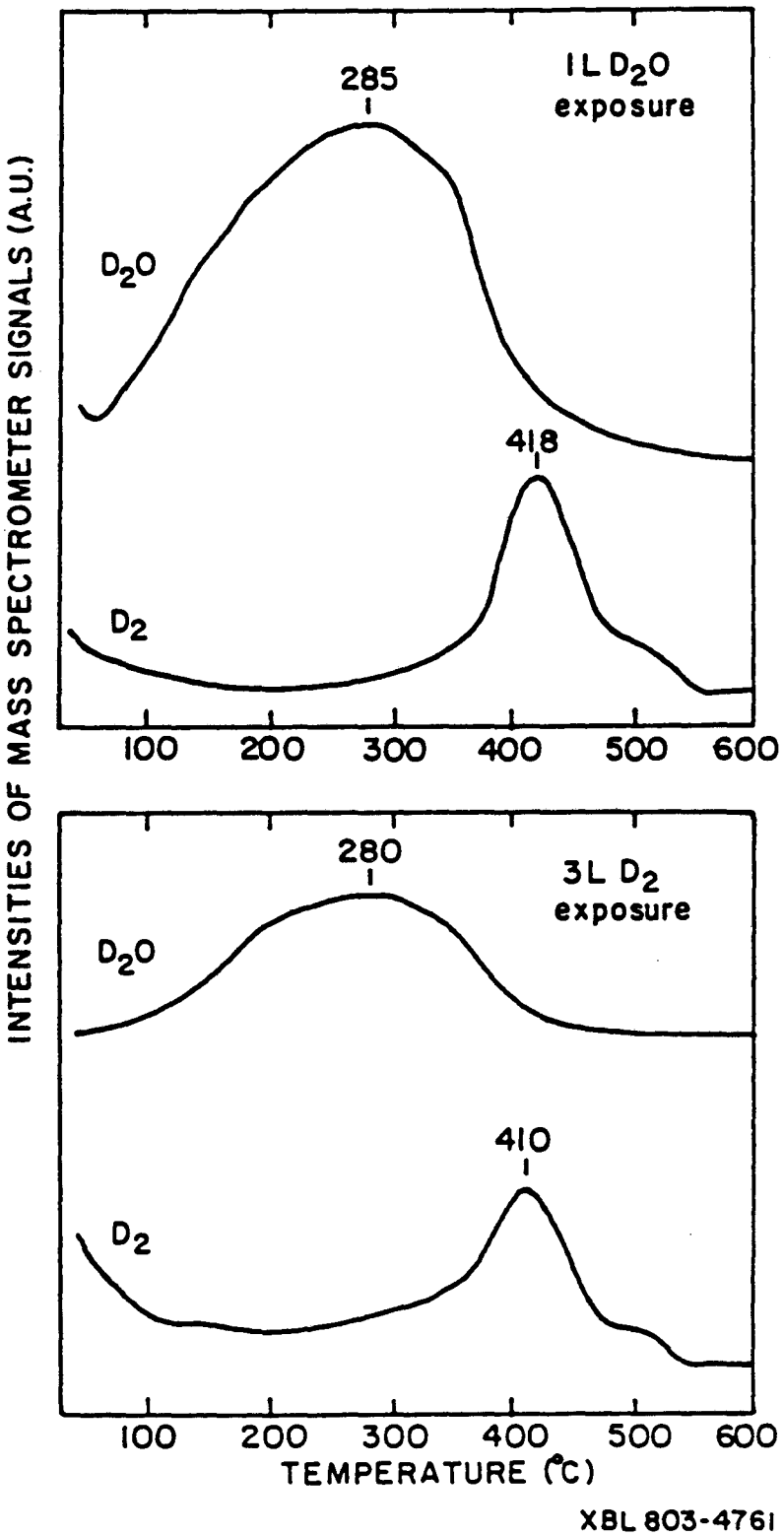
285
1 L D_2O exposure
D_2O
418
D_2
100
200
300
400
500
600
280
3L D_2 exposure
D_2O
410
D_2
100
200
300
400
500
600
INTENSITIES OF MASS SPECTROMETER SIGNALS (A.U.)
TEMPERATURE (°C)
XBL 803-4761

Fig. 9

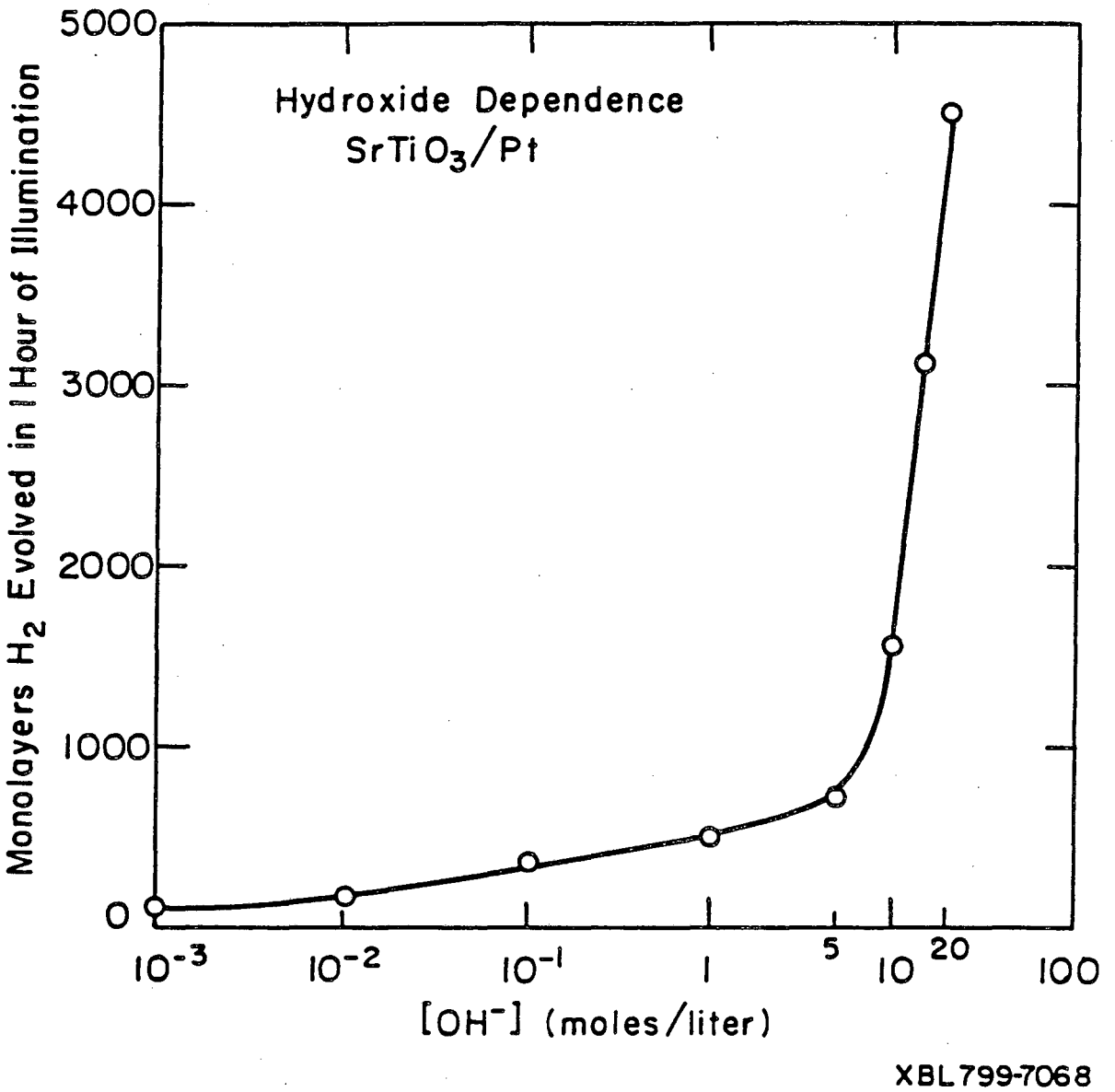
Hydroxide Dependence
SrTiO3/Pt
Monolayers H2 Evolved in 1 Hour of Illumination
5000
4000
3000
2000
1000
0
10-3
10-2
10-1
1
5
10
20
100
[OH-] (moles/liter)
XBL799-7068

Fig. 10

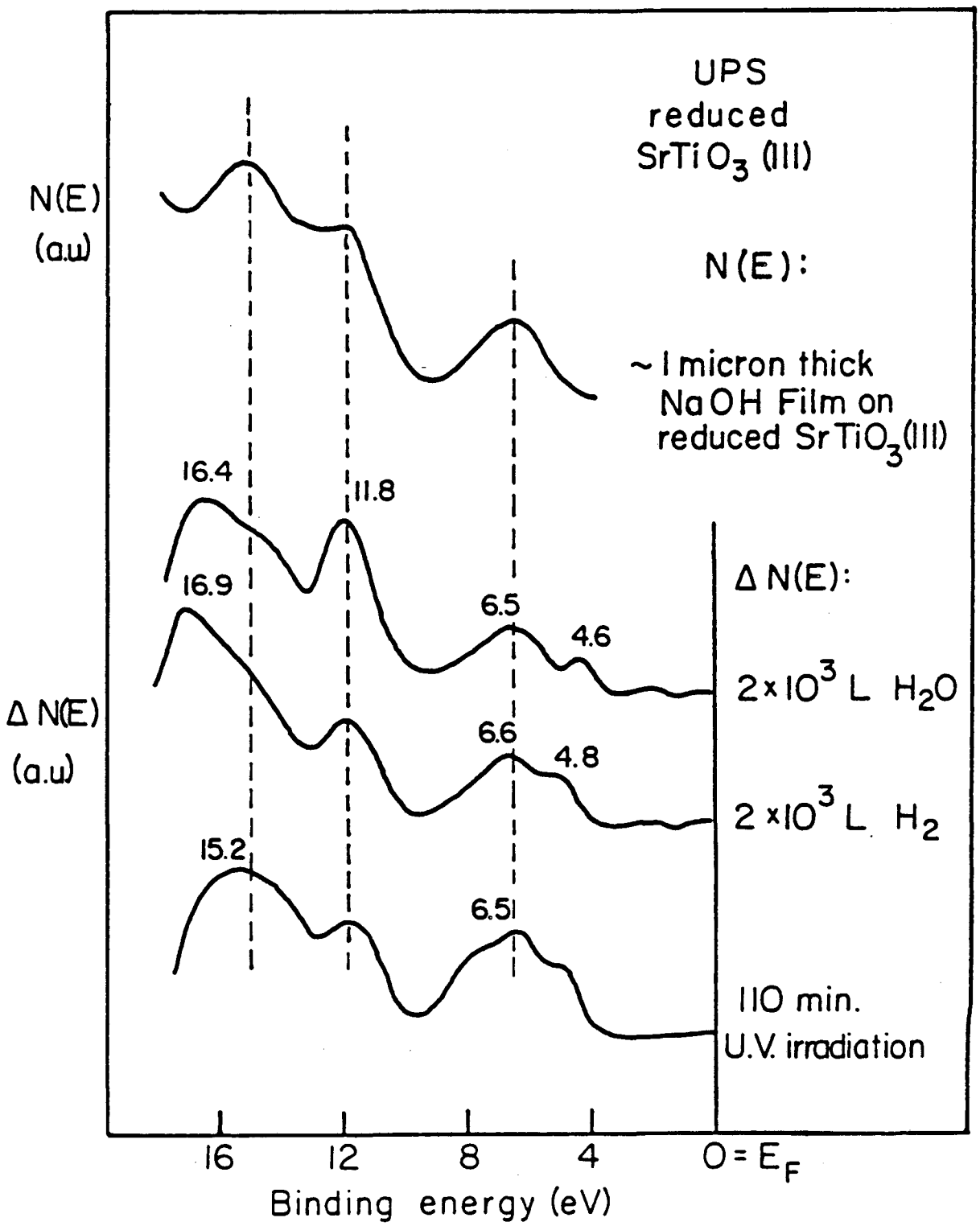

XBL 799-7042

Fig. 11

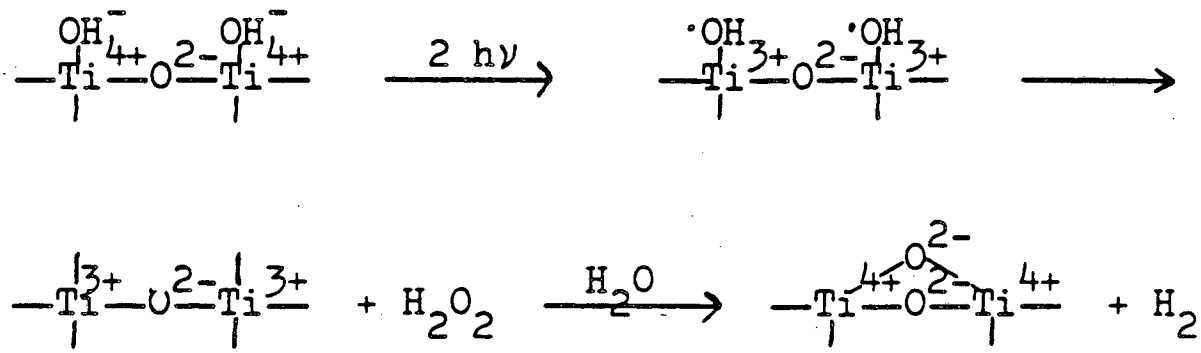

Van Damme and Hall, JACS 101 4373

XBL 822-7816

Fig. 12

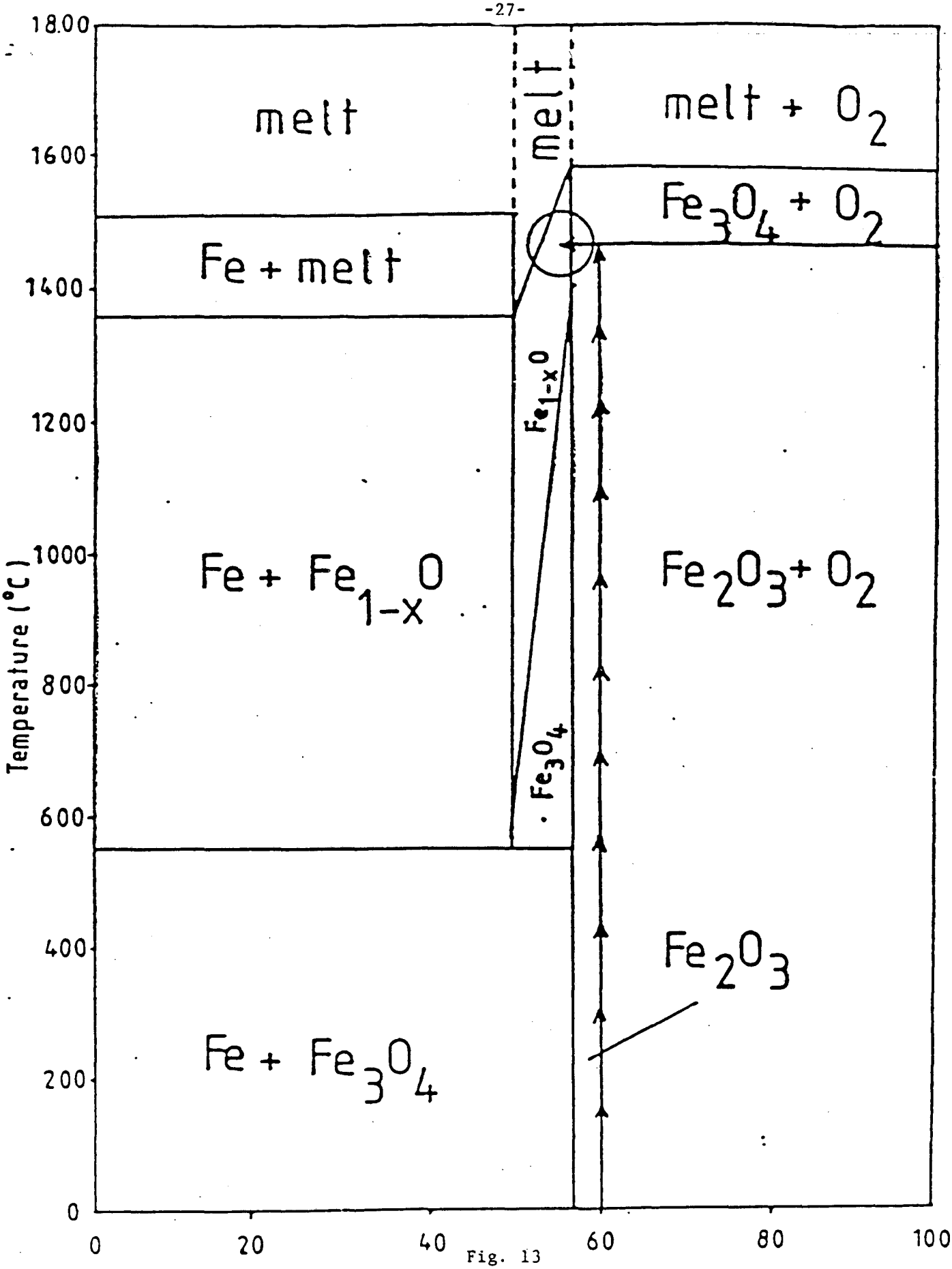
melt
melt
melt + O2
Fe3O4 + O2
Fe + melt
Fe1-xO
Fe + Fe1-xO
Fe2O3+ O2
Fe3O4
Fe2O3
Fe + Fe3O4
Temperature (°C)
18.00
1600
1400
1200
1000
800
600
400
200
0
0
20
40
60
80
100
Atomic Percent Oxygen

Fig. 13

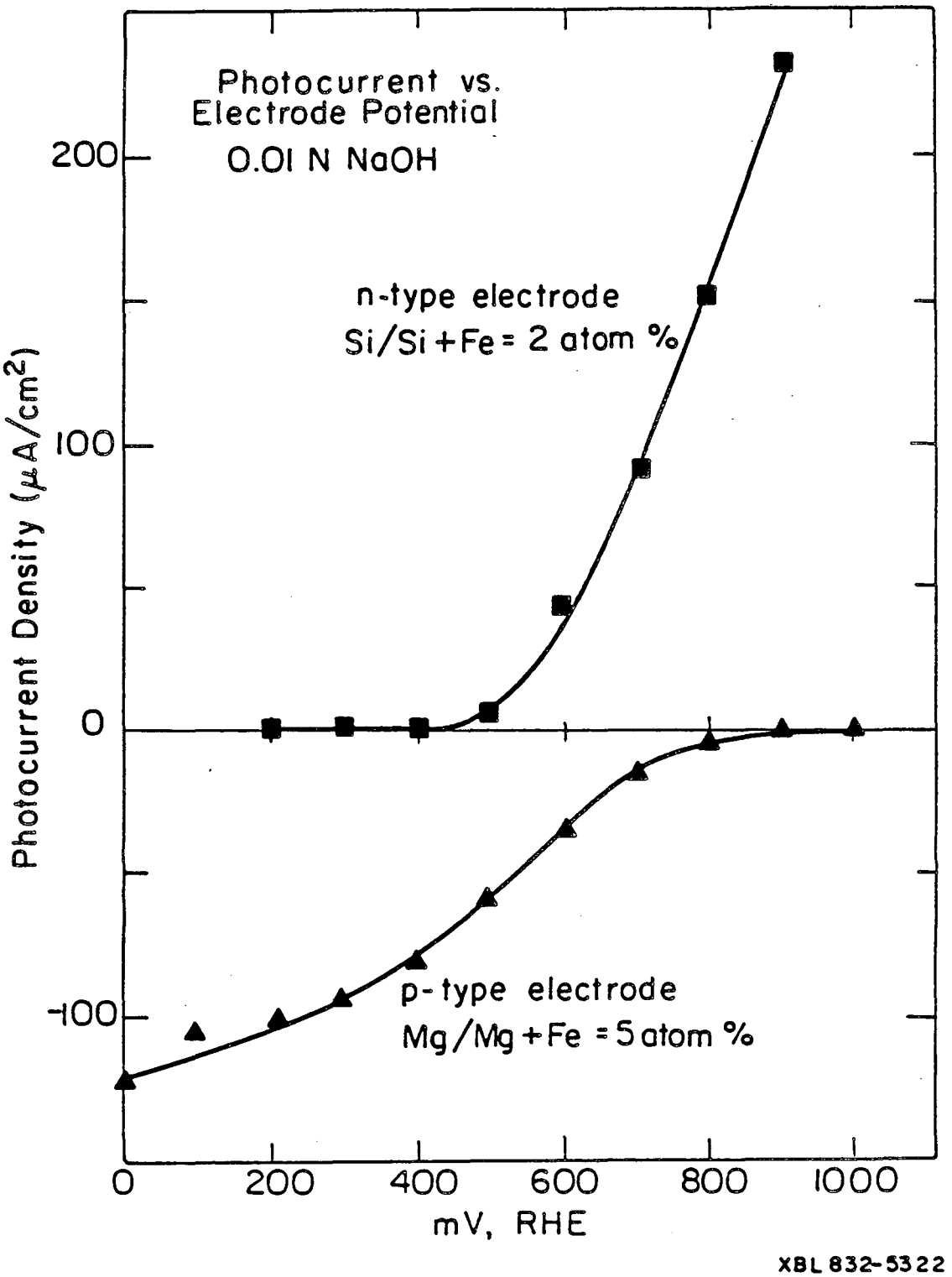
Photocurrent vs.
Electrode Potential
0.01 N NaOH
n-type electrode
Si/Si+Fe = 2 atom %
p-type electrode
Mg/Mg+Fe = 5 atom %
Photocurrent Density (μA/cm²)
200
100
0
-100
0
200
400
600
800
1000
mV, RHE
XBL 832-5322

Fig. 14

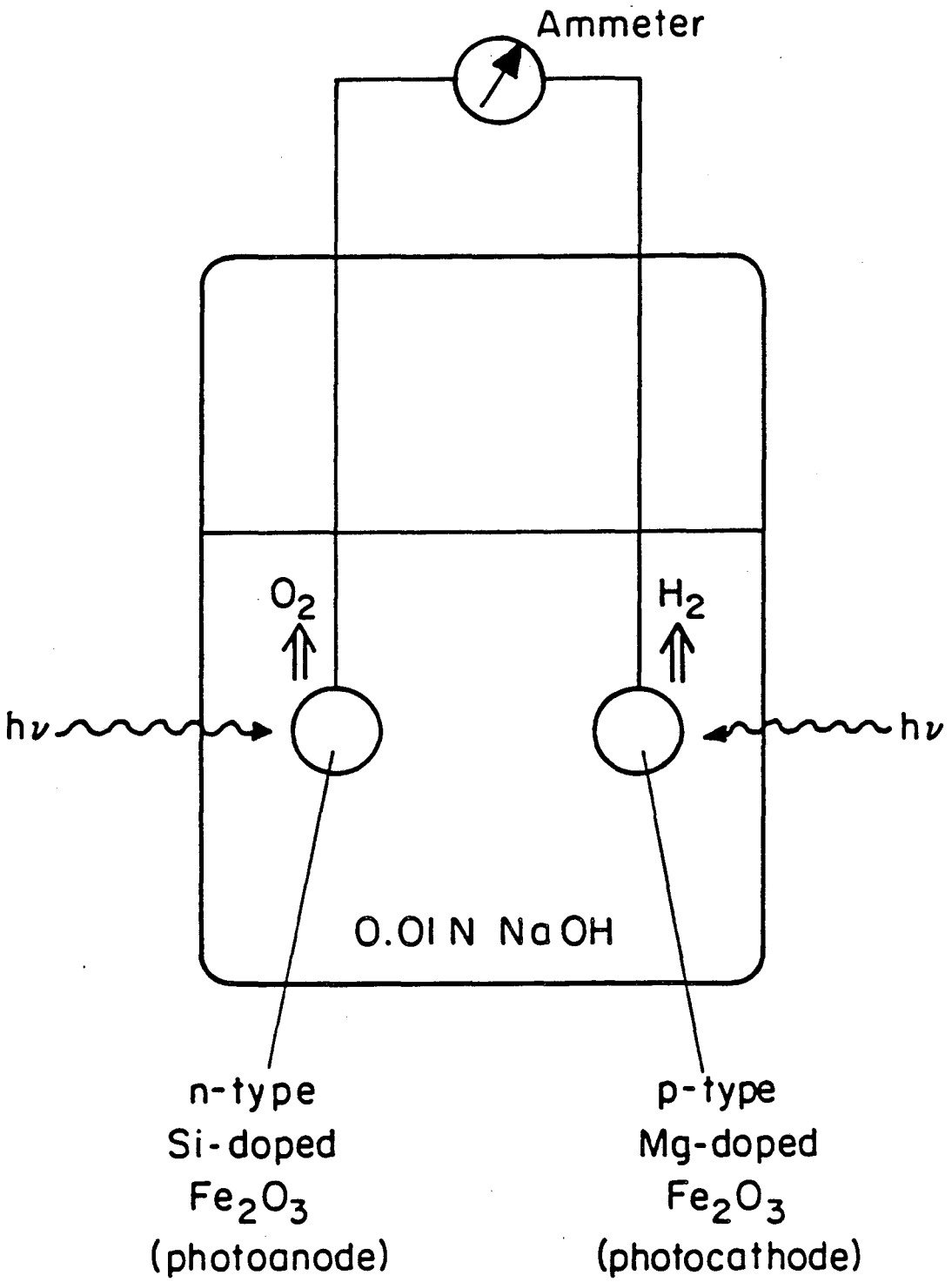
Ammeter
O_2
H_2
hν
hν
0.01 N NaOH
n-type
Si-doped
Fe_2O_3
(photoanode)
p-type
Mg-doped
Fe_2O_3
(photocathode)
XBL 835-5725

Fig. 15

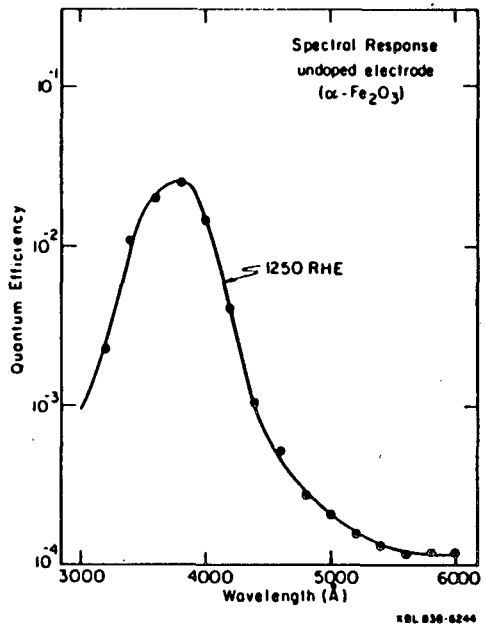
Spectral Response
undoped electrode
(α-Fe2O3)
1250 RHE
Quantum Efficiency
Wavelength (Å)
3000
4000
5000
6000

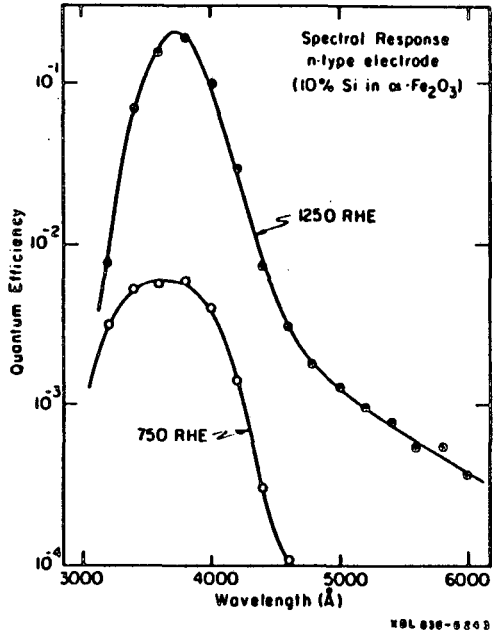
Spectral Response
n-type electrode
(10% Si in α-Fe2O3)
1250 RHE
750 RHE
Quantum Efficiency
Wavelength (Å)
3000
4000
5000
6000

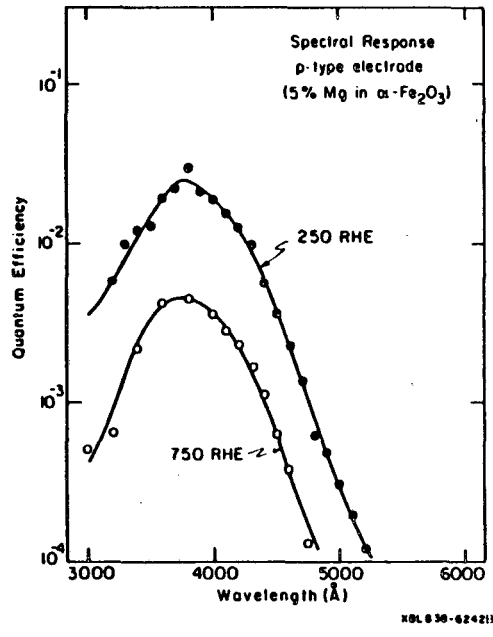
Spectral Response
p-type electrode
(5% Mg in α-Fe2O3)
250 RHE
750 RHE
Quantum Efficiency
Wavelength (Å)
3000
4000
5000
6000

Fig. 16

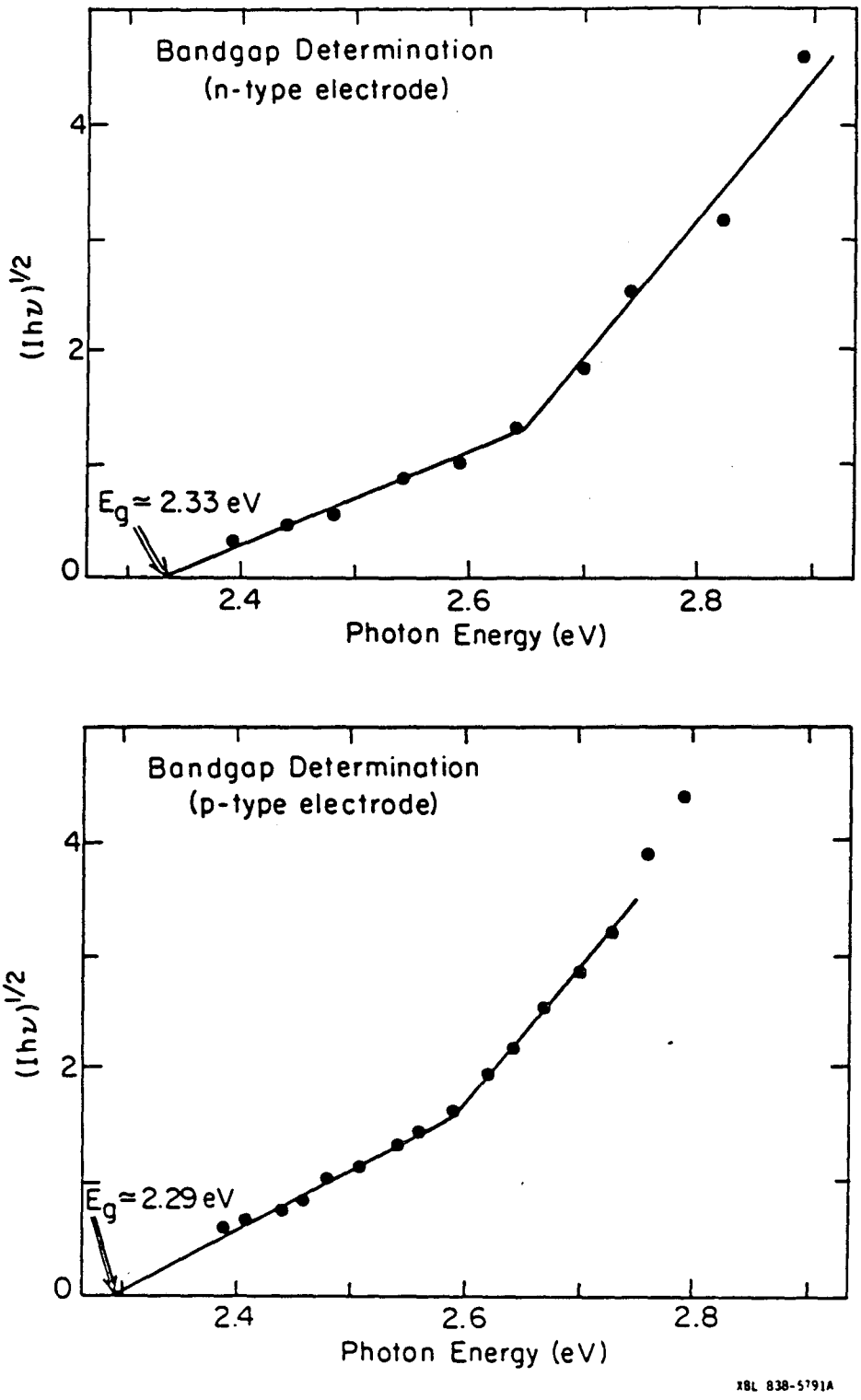
Bandgap Determination
(n-type electrode)
$E_g \simeq 2.33$ eV
$(Ih\nu)^{1/2}$
Photon Energy (eV)
0
2
4
2.4
2.6
2.8
Bandgap Determination
(p-type electrode)
$E_g \simeq 2.29$ eV
$(Ih\nu)^{1/2}$
Photon Energy (eV)
XBL 838-5791A

Fig. 17

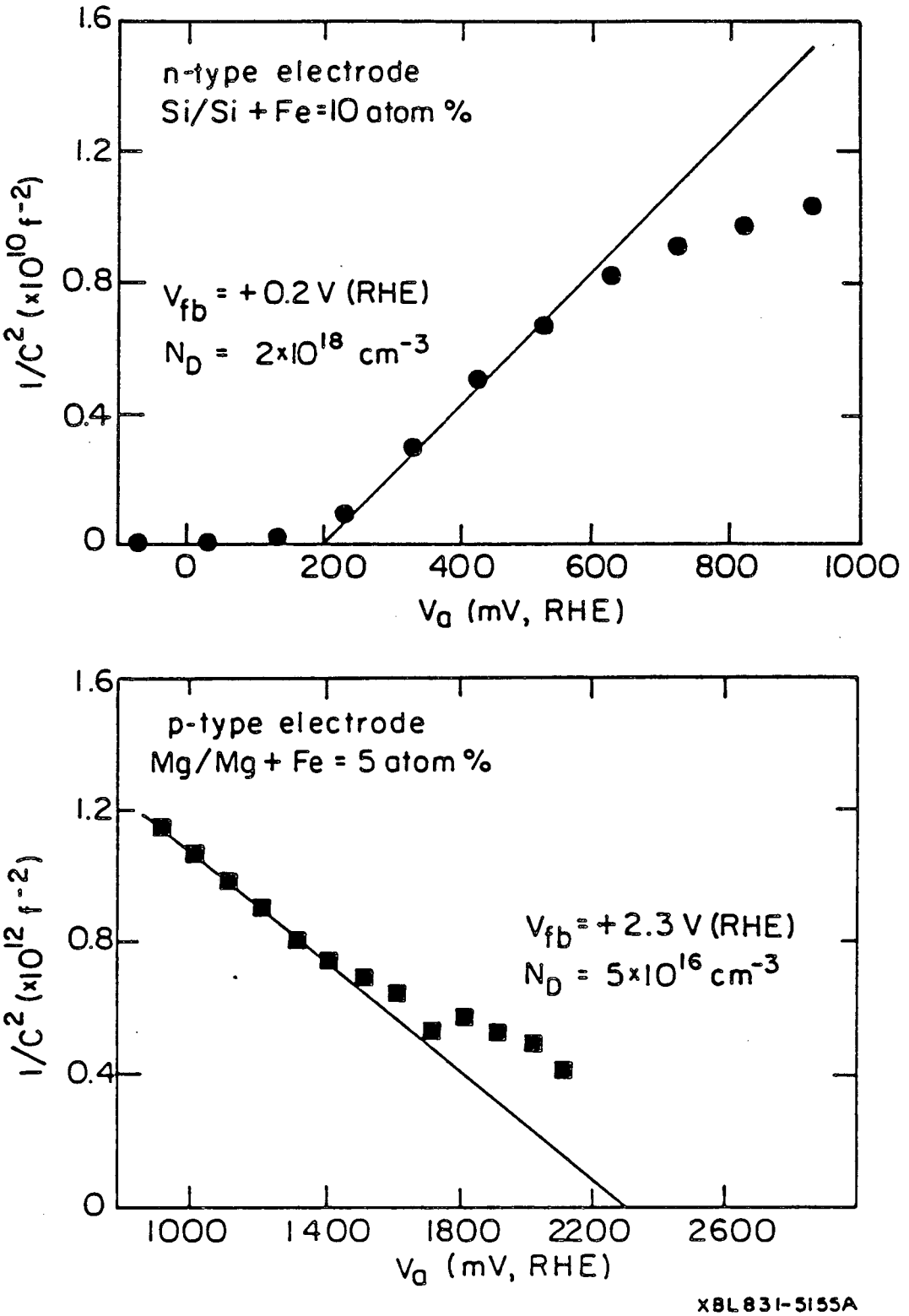
n-type electrode
Si/Si + Fe=10 atom %
V_{fb} = +0.2 V (RHE)
N_D = 2×10^{18} cm^{-3}
1/C^2 (×10^{10} f^{-2})
1.6
1.2
0.8
0.4
0
0
200
400
600
800
1000
V_a (mV, RHE)
p-type electrode
Mg/Mg + Fe = 5 atom %
V_{fb} = +2.3 V (RHE)
N_D = 5×10^{16} cm^{-3}
1/C^2 (×10^{12} f^{-2})
1.6
1.2
0.8
0.4
0
1000
1400
1800
2200
2600
V_a (mV, RHE)
XBL831-5155A

Fig. 18

ENERGETICS OF CONNECTED P-TYPE AND N-TYPE IRON OXIDES

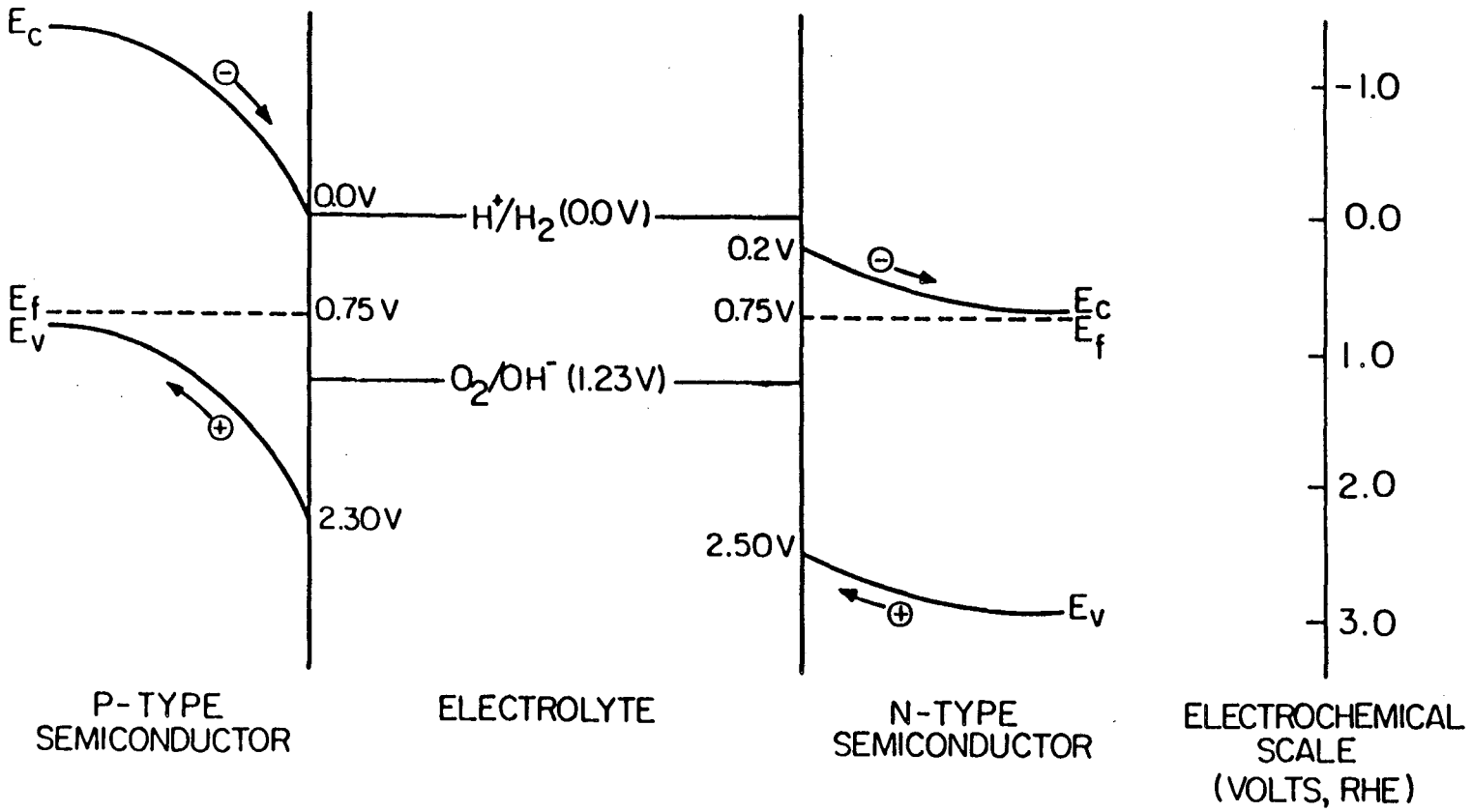

XBL 832-5181A

Fig. 19

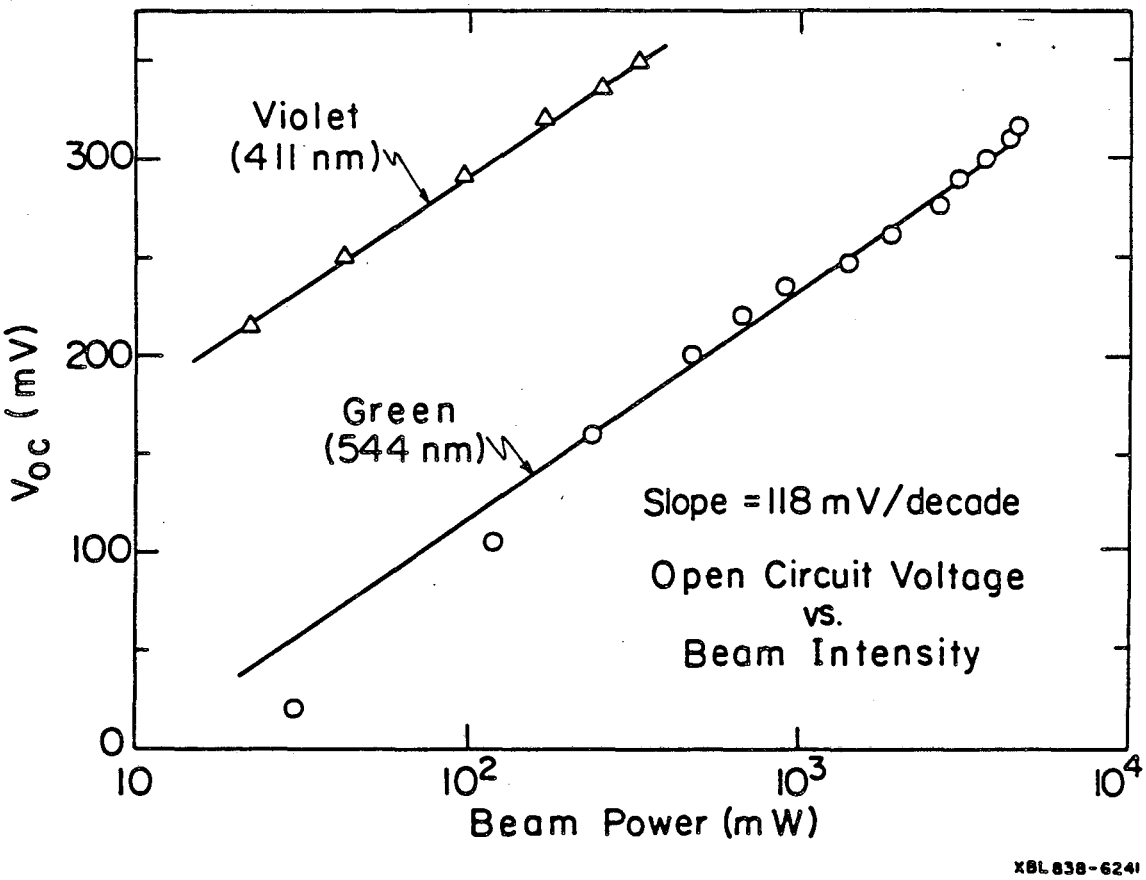
Violet
(411 nm)
Green
(544 nm)
Slope = 118 mV/decade
Open Circuit Voltage
vs.
Beam Intensity
V_{oc} (mV)
300
200
100
0
10
10^2
10^3
10^4
Beam Power (mW)
XBL838-6241

Fig. 20

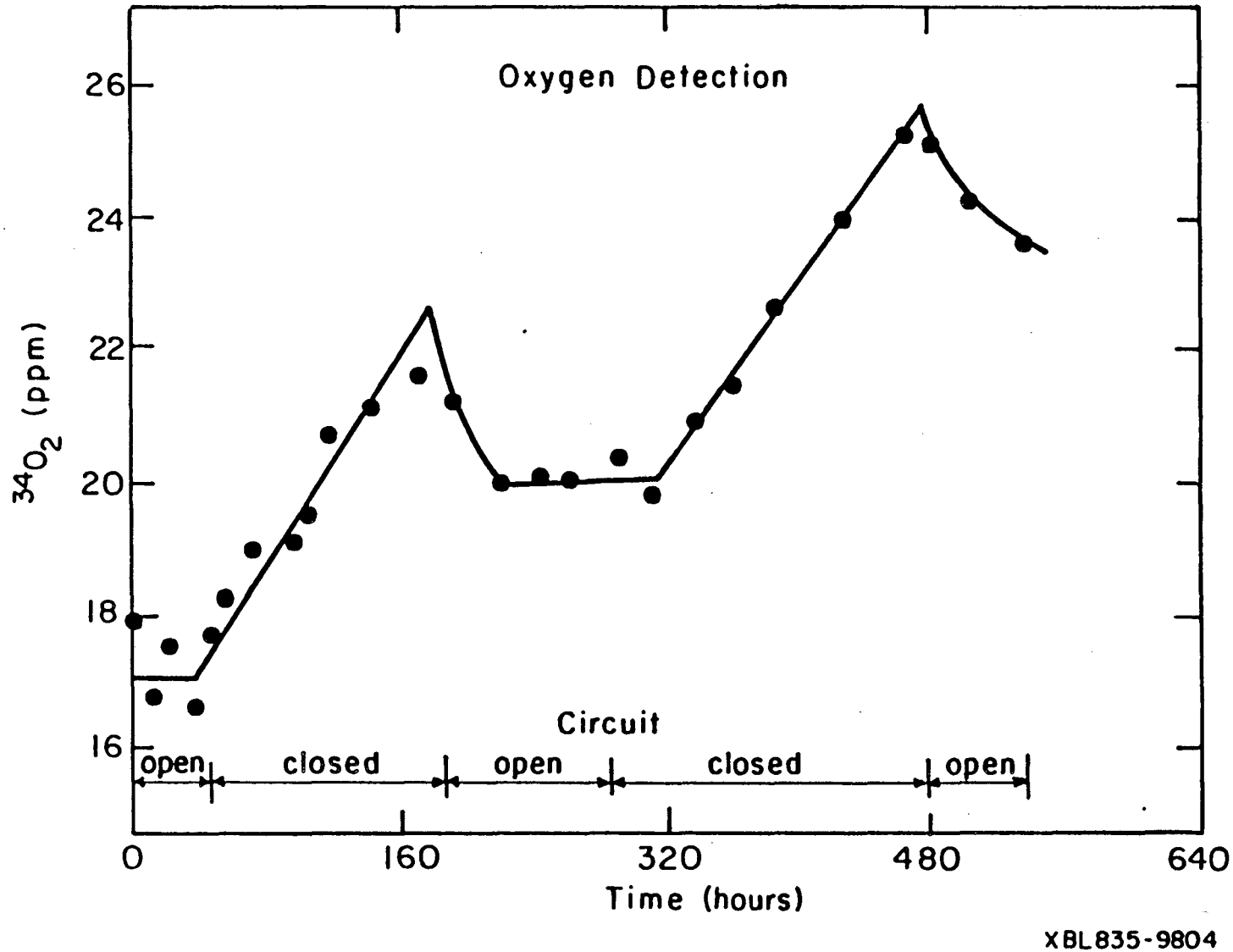
Oxygen Detection
$^{34}O_2$ (ppm)
26
24
22
20
18
16
Circuit
open
closed
open
closed
open
0
160
320
480
640
Time (hours)
XBL835-9804

Fig. 21

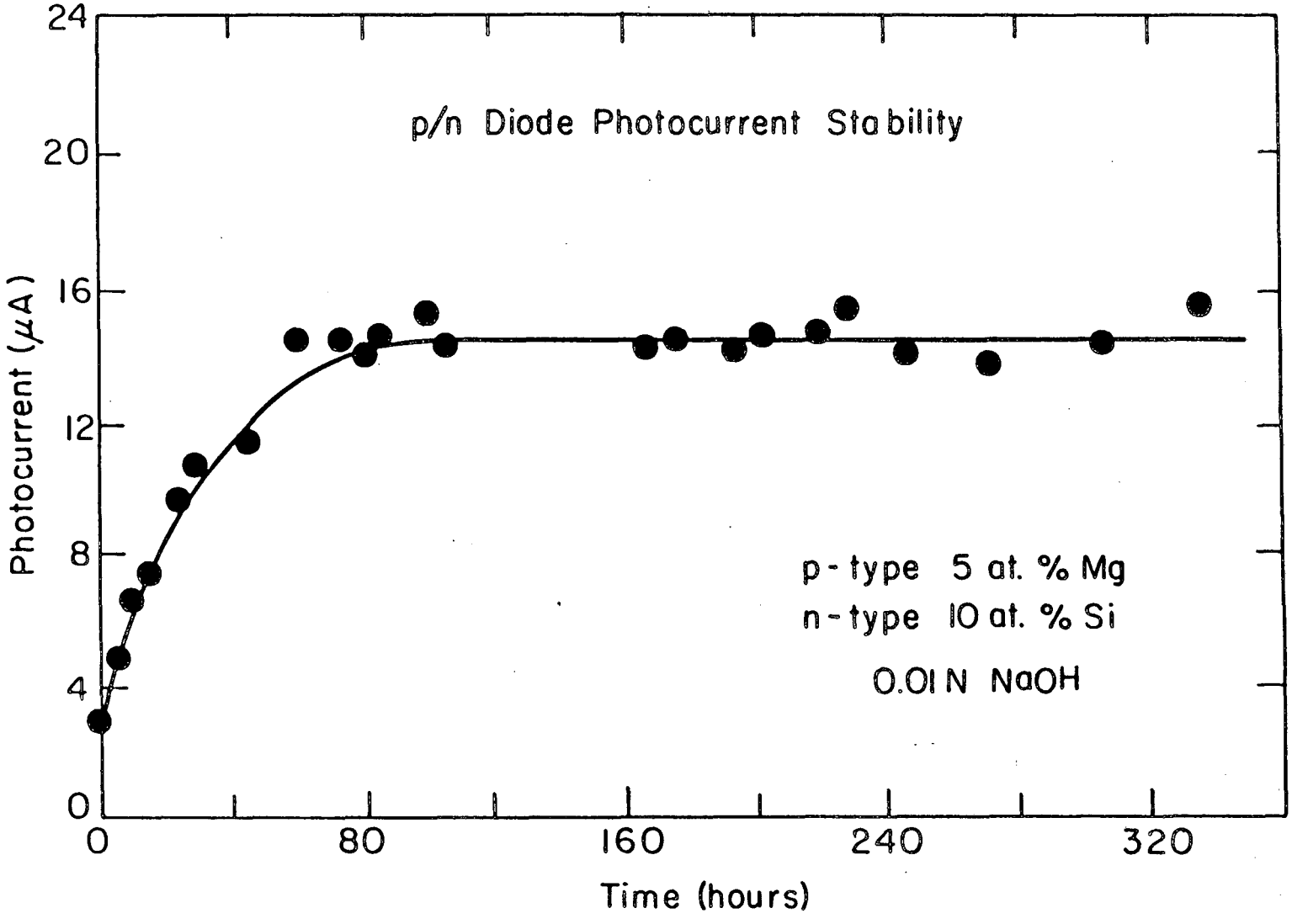

XBL 833-8744

Fig. 22

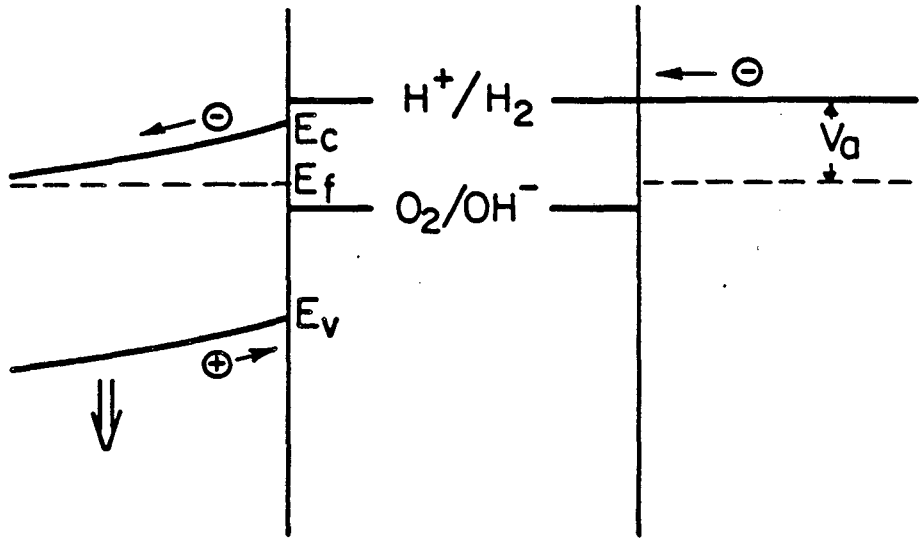

(A)

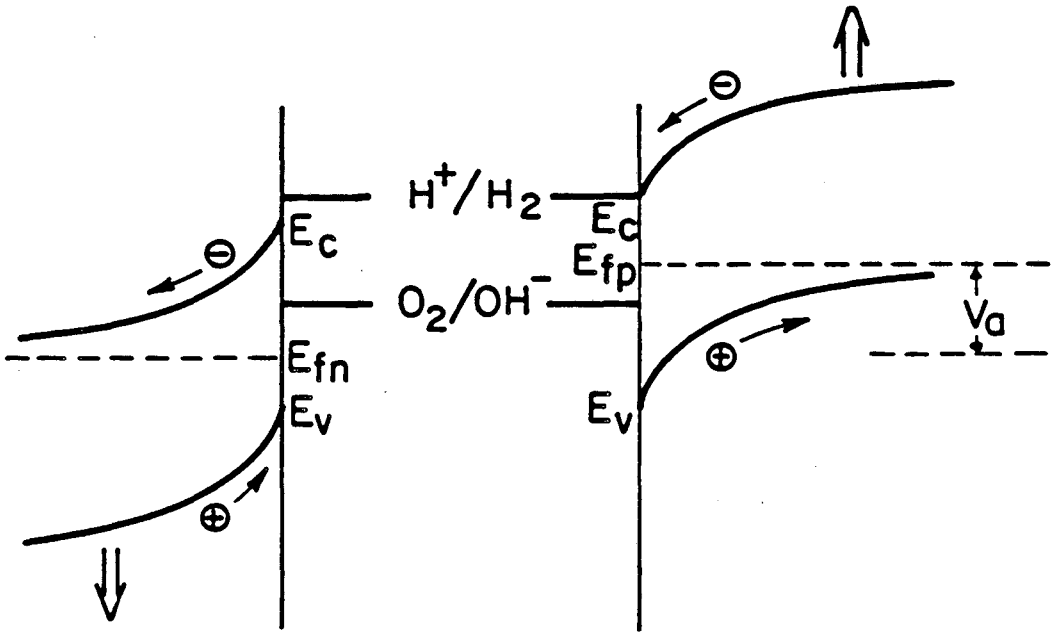

(B)

XBL 838-6164

Fig. 23

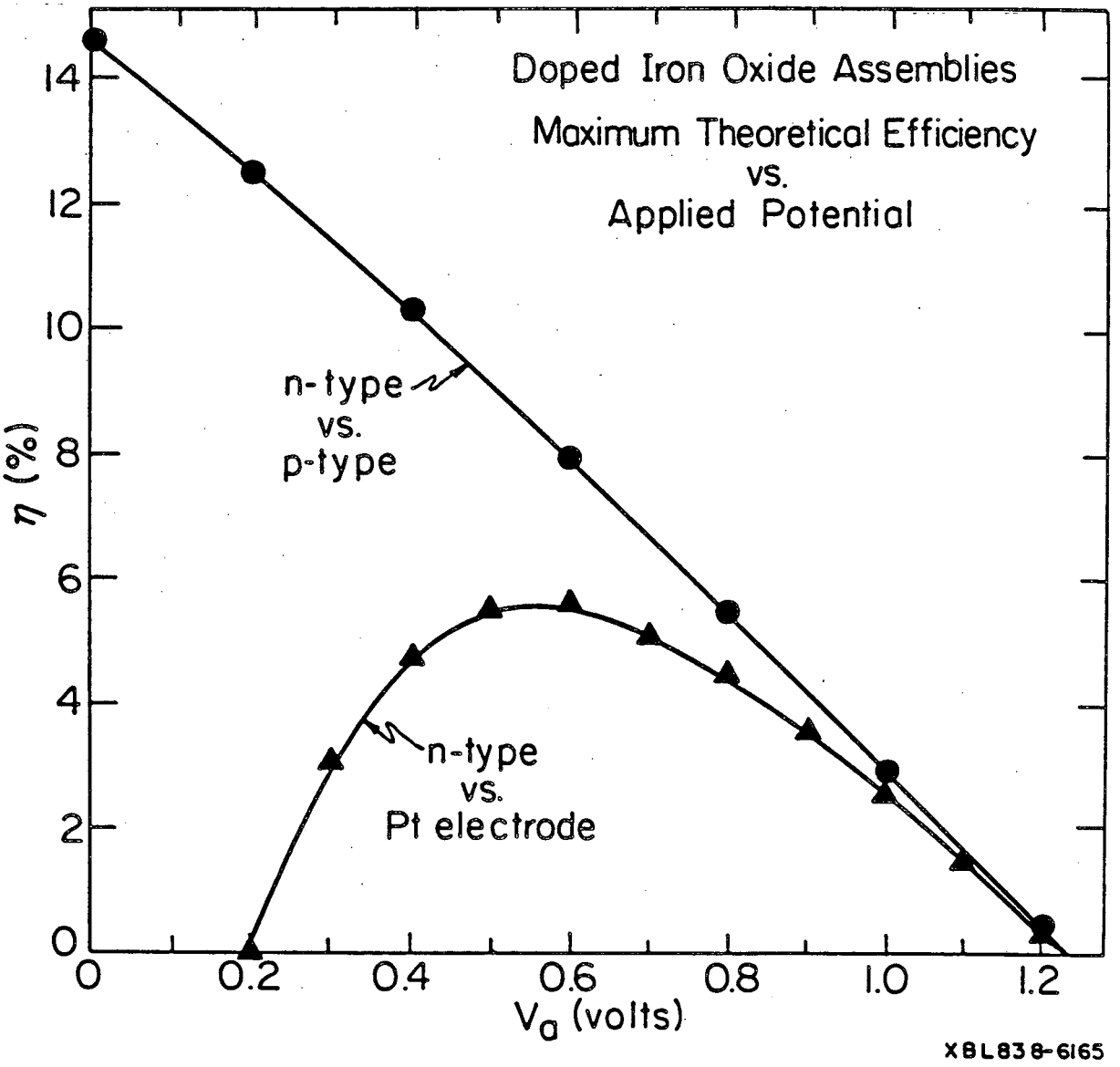
Doped Iron Oxide Assemblies
Maximum Theoretical Efficiency
vs.
Applied Potential
n-type
vs.
p-type
n-type
vs.
Pt electrode
η (%)
0
2
4
6
8
10
12
14
0
0.2
0.4
0.6
0.8
1.0
1.2
V_a (volts)
XBL838-6165

Fig. 24

A. Hydrogen production from $SrTiO_3$ crystals covered by thick (>30μ) NaOH films saturated with water vapor

Crystal	Monolayers* H_2/hr
Pre-reduced, platinized	1580
Pre-reduced, metal-free	100
Stoichiometric, metal-free	30

B. Hydrogen production from $SrTiO_3$ crystals in 20 M NaOH

Crystal	Monolayers* H_2/hr
Pre-reduced, platinized	4500
Stoichiometric, platinized	120
Pre-reduced, metal-free	30
Stoichiometric, metal-free	50
Pre-reduced, gold coated	200

*1 monolayer $\equiv 1 \times 10^{15}$ molecules/cm^2 illuminated surface

Table 1

This report was done with support from the Department of Energy. Any conclusions or opinions expressed in this report represent solely those of the author(s) and not necessarily those of The Regents of the University of California, the Lawrence Berkeley Laboratory or the Department of Energy.

Reference to a company or product name does not imply approval or recommendation of the product by the University of California or the U.S. Department of Energy to the exclusion of others that may be suitable.

LAWRENCE BERKELEY LABORATORY
TECHNICAL INFORMATION DEPARTMENT
UNIVERSITY OF CALIFORNIA
BERKELEY, CALIFORNIA 94720